ELSEVIER

Solid State Nuclear Magnetic Resonance 9 (1997) 277–301

SOLID STATE
Nuclear Magnetic
Resonance

The role of polarization of Xe by di- and monovalent cations in ^{129}Xe NMR studies in zeolite A [1]

Cynthia J. Jameson [a,*], Hyung-Mi Lim [a], A. Keith Jameson [b]

[a] *Department of Chemistry, University of Illinois at Chicago, 845 W. Taylor, Chicago, IL 60607-7061, USA*
[b] *Department of Chemistry, Loyola University, Chicago, IL 60626, USA*

Received 14 April 1997; accepted 4 August 1997

Abstract

We consider the role of polarization in the adsorption of Xe in zeolites of type A by direct comparative analysis of the adsorption isotherms, distributions of occupancies, and ^{129}Xe NMR chemical shifts of Xe_n in cages containing Ca_xNa_{12-2x} ions per alpha cage ($x = 0, 1, 2, 3, 5$). We find that the qualitative trends in the adsorption isotherms, and in the progressions of Xe_n chemical shifts (for $n = 0$–8 in cages with $x = 0$, 1 Ca^{2+} ions and for $n = 0$–5 in cages with $x = 2$, 3 Ca^{2+} ions) upon increasing the level of Ca^{2+} ion for Na^+ ion substitution could only be accounted for by including polarization of the Xe atom by the zeolite framework and its ions. This system, which permits observation of individual Xe_n peaks and of directly comparable adsorption isotherms in several cage types, provides a good model system for the interpretation of the more general case in which only the overall average ^{129}Xe NMR chemical shift is observed in open network zeolites, arising from free exchange of Xe among cavities of variable occupancy and variable cation distribution. © 1997 Elsevier Science B.V.

Keywords: Xenon; Zeolite NaA; Adsorption; Ca ion exchange; Polarization energy

1. Introduction

The properties of zeolites in adsorption and catalysis are significantly influenced by the number and nature of exchangeable cations [1–3]. The number of exchangeable cations is determined by the Si/Al ratio in the zeolite framework. The pioneering work of Engelhardt et al. established the method of determining the Si/Al ratio from the ^{29}Si chemical shifts in the MAS NMR spectra of zeolites [4,5]. Starting from the first paper by Fraissard and Ito in 1982 [6], ^{129}Xe NMR spectroscopy is now a standard technique in the study of zeolite and other solid materials. In zeolites the ^{129}Xe chemical shift is known empirically to depend on zeolite pore and channel dimensions, on its Al/Si ratio, on cation distribution and location of cations, on co-adsorbed molecules, dispersed metal atoms, or paramagnetic ions, on blockage of pores, and on domains of different composition or crystallinity [7–9]. In all these applications the large variations in the Xe chemical shifts that are observed offer the tantalizing possibility that Xe NMR can be used in a quantitative a priori fashion in the characterization of solid materials.

* Corresponding author.

[1] Dedicated to Günter Engelhardt on the occasion of his 60th birthday.

This is yet to be realized. The mobility of the Xe atoms is such that only one Xe signal is usually observed in the NMR spectrum; the average chemical shift of the single peak under fast exchange and its dependence on the temperature and coverage are all that can be measured in nearly all these applications. Convoluted into the chemical shift of this one peak are all manner of distributions, residence times, and the chemical shift functions for the various atoms or ions with which the Xe interacts.

Of particular interest is the dependence of the Xe chemical shift on the Al/Si ratio, the types and the distribution of the cations. The dependence of the Xe chemical shift on the Al/Si ratio has been documented in the faujasites [10,11]. Furthermore, a series of very carefully executed experiments have established quantitatively the changes in the ^{129}Xe chemical shift $\delta(^{129}\mathrm{Xe})$ of Xe in the limit of zero Xe loading, $\lim \langle n \rangle_{\mathrm{Xe}} \rightarrow 0$ $\delta(^{129}\mathrm{Xe})$, as Na^+ ions are exchanged with K^+, Rb^+, Cs^+, Mg^{2+}, Ca^{2+}, Sr^{2+}, Ba^{2+}, Zn^{2+}, Co^{2+}, Ni^{2+}, Cu^{2+}, etc. in zeolite Na*Y* [12,13], and as Ca^{2+} ions are exchanged with Na^+ ions in Na*A* [14]. These papers also reported well-documented quantitative changes in the slopes, $\partial\delta(^{129}\mathrm{Xe})/\partial\langle n \rangle_{\mathrm{Xe}}$, of the ^{129}Xe chemical shifts as a function of average Xe occupancy $\langle n \rangle_{\mathrm{Xe}}$ upon cation exchange. We believe that several factors contribute to these observed changes. The effect of exchanging the cation on the average chemical shift of Xe in fast exchange in a zeolite has to do, in part, with a change in the excluded volume (a larger cation leaves a smaller effective volume over which the Xe–Xe interactions can operate). Another part has to do with the different polarizabilities of the cations, leading to different well-depths in the potential function between the Xe and the cation, thereby altering the one-body distribution of the Xe in the cage. Both of these factors affect the nature of the averaging over the various positions of the Xe atom within the zeolite and thus, lead to a change in the average ^{129}Xe NMR chemical shift. Finally, part of the observed changes has to do with the differences between the ^{129}Xe shielding function itself for a Xe atom interacting with a Na^+ ion as opposed to a Xe atom interacting with a Cs^+ ion, for example. Although these experiments were very carefully done and the results are quantitative and internally consistent and generally not inconsistent with other known information about Xe adsorption in zeolites, a quantitative interpretation is hampered by cation disorder in the faujasites. The extent of cation replacement can be determined (by chemical analytical procedures), but there is no independent way of finding out the statistical distribution of the exchanged ions among the sites, leading to a disordered crystal structure. Where do cations go when they are exchanged? There is some hard evidence on cation site occupancies in the ^{23}Na NMR results of Engelhardt in Na*Y*, [15] and of the cation migration in zeolite LaNa*Y*, [16] but very little else in the way of direct evidence. The Xe NMR chemical shift is the commonly used method of characterization of cation-exchanged zeolites. Since the ^{129}Xe chemical shift is completely averaged over the distribution of Xe atoms in such environments, the quantitative interpretation of these comprehensive experimental data via grand canonical Monte Carlo (GCMC) or molecular dynamics simulations may be compromised by the problems associated with cation disorder as well as varying Si/Al ratio.

If the ^{129}Xe chemical shift is to be used as a probe of cation-exchanged zeolites, we need to have a fundamental understanding of the effects of cation size and location on the Xe chemical shift. In our attempts to contribute to a fundamental understanding of Xe as a probe of these systems, we have used the Xe in zeolite *A* as a model system [17,18]. In the same way that the observation of the individual Xe_n clusters in Na*A* provided more detailed information about the distribution of atoms in zeolite cavities and the average chemical shifts for different numbers of Xe atoms in a cavity than was possible from the ^{129}Xe NMR studies of zeolites under fast exchange, the study of Xe_n clusters in various ion-exchanged *A*-type zeolites should provide the fine details that are required to sort out the various factors affecting Xe chemical shifts in ion-exchanged zeolites in general. We reported for the first time the observation of the individual peaks corresponding to the Xe_n clusters trapped in zeolite K*A*, and their temperature dependence [19]. Since the replacement of Na^+ by K^+ is complete in K*A*, there is no ambiguity about the cation site occupancies. By comparison of the individual Xe_n clusters in K*A* with those in Na*A*, we have obtained direct information on the effect of the cation on the Xe chemical shift. GCMC simula-

tions of Xe in K *A* compared to Xe in Na *A*, provide detailed information about the effects of the type of cation on the Xe one-body distribution function, the effects of the cation type on the ^{129}Xe chemical shift of the single Xe in an alpha cage, and the separate effects of the larger excluded volume as reflected in the changes in the Xe–Xe pair distribution functions, the changes in the Xe_n chemical shifts, and the changes in the Xe_n–Xe_{n-1} incremental shifts, all of which were tested against experiment. We can generalize these cation effects to help provide an understanding of the average Xe chemical shift observed under fast exchange in various cation-exchanged zeolites. In another experiment, we have studied the ^{129}Xe NMR spectra under magic angle spinning (MAS) of Xe_n in zeolite Na *A* that had been dehydrated subsequent to very low levels of Ca^{2+} ion exchange [20]. We observed the effects of very low levels of substitution of Ca^{2+} ion for Na^+ in a high-resolution spectrum of Xe_n clusters, with each type of cage providing its own progression of Xe_n peaks. At first, we observed two Xe_n progressions, with different $\langle n \rangle_{Xe}$. With increasing level of Ca^{2+} ion exchange the second Xe_n set grows in intensity and yet other sets of easily assigned Xe_n peaks appear, in progressions systematically growing in intensity upon increasing Ca substitution. The advantage of these studies is that the intensities and the chemical shifts of the Xe_n peaks belonging to the same type of cage can be characterized independently of the other types of cages. Furthermore, unlike the faujasites, the Si/Al ratio remains fixed at 1.0 and the divalent ions have only one type of site (in the middle of the 6-rings) in the cages of zeolite *A*. In contrast to previous attempts by others to use Xe in fast exchange to probe structural changes in zeolites, our ability to observe entire progressions of Xe_n cluster peaks puts strict constraints on the interpretation since the effects can be examined in each Xe_n cluster, in each progression. In this paper, we describe the experimental findings and provide a quantitative interpretation of the observations in the $Ca_xNa_{12-2x}A$ system using grand canonical Monte Carlo simulations. We shall find that this system provides a paradigm for the contributions of polarization of the Xe atom to the observed adsorption properties of Xe in zeolites and about the way in which cation type and position affects the ability of Xe to provide information via its NMR chemical shifts.

2. The experimental results

The MAS NMR spectra of Xe in pure $Na_{12}A$ zeolite from Edith Flanigen show only the one progression of Xe_n peaks, [20] previously observed in the static NMR spectra of the same sample, but with dramatically reduced line widths. The structure of this zeolite is represented in Fig. 1, based on the refined X-ray diffraction results of Pluth and Smith [21]. After various levels of Ca^{2+} exchange, in which one Ca^{2+} ion is substituted for two Na^+ ions, what is the nature of the cation distribution in the dehydrated zeolite?

The MAS spectra provide detailed information about the nature of very low levels of Ca^{2+} ion substitution. Additional progressions of Xe_n peaks appear and grow in as the Ca^{2+} content of the zeolite is increased. The relative intensities and the chemical shifts of the Xe_n peaks lead to the follow-

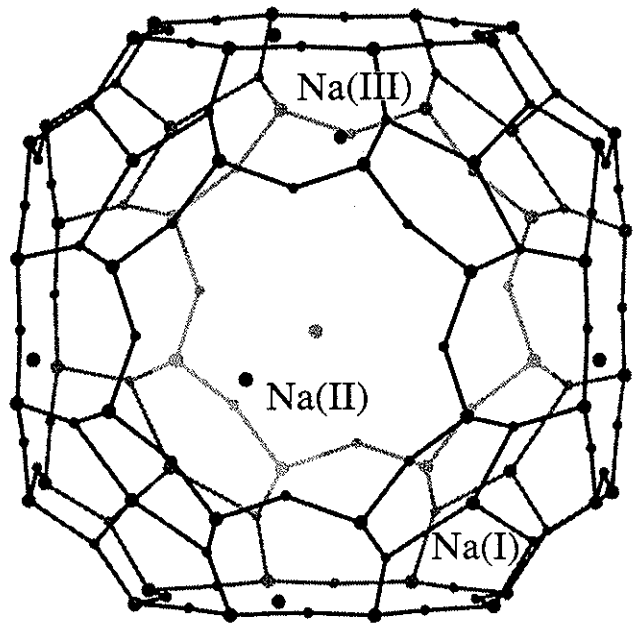

Fig. 1. Three cation site types in an alpha cage of zeolite Na *A*. Si and Al atoms alternate to give Si/Al = 1.0. The 4-, 6-, and 8-rings are comprised of these numbers of bridging oxygen atoms. The Na^+ ion in the unique site is Na(III), located off-center inside the alpha cage, coordinated to a 4-ring. Na(I) sites are at the centers of 6-rings and Na(II) sites are off-center in the plane of the 8-ring windows.

Table 1
The experimental chemical shifts (ppm) of the Xe_n peaks assigned to $Ca_0Na_{12}A$, $Ca_1Na_{10}A$, Ca_2Na_8A, and Ca_3Na_6A, relative to $Ca_0Na_{12}A$ (pure Na A) (inconclusive, for intensities too weak to provide a good deconvolution of the composite peak)

	$Ca_1Na_{10}A$	Ca_2Na_8A	Ca_3Na_6A
Xe_1	−3.1	+4.3	+8.4
Xe_2	−3.0	+2.8	+7.8
Xe_3	−2.7	+2.3	+7.3
Xe_4	−3.1	+2.0	+6.8
Xe_5	−3.6	+1.1	~ +6
Xe_6	−4.6	Inconclusive	Inconclusive
Xe_7	−4.4	–	–

ing conclusions: (a) It is clear that exchange of Ca^{2+} for $2Na^+$ ions gives rise to the simultaneous existence of cages with differing numbers of Ca^{2+} ions. Rather than uniform substitution in all cages we have a distribution of Ca^{2+} among the cages. (b) At low Ca numbers, Ca^{2+} substitution does not appear to lead to the opening up of a window (which would result from substitution of Ca^{2+} for a Na(II) ion in an 8-ring window and one other Na^+ ion). If a substantial fraction of the Na(II) ions had been removed, fast exchange of Xe through open windows would have been observed. (c) The first extra set of peaks that may be attributed to Ca^{2+} substitution have a uniform shift of all Xe_n clusters to a lower ^{129}Xe chemical shift, whereas further Ca^{2+} substitution creates cages with Xe_n clusters at higher chemical shifts, suggesting that the first Ca^{2+} substitution is qualitatively different from subsequent ones. This is consistent with the first Ca^{2+} ion taking the place of one Na(III) and one Na(I) in an alpha cage. (d) From the observed coexistence of cages with differing numbers of Ca^{2+} ions, it is possible to determine the distribution of cage types from the overall intensities. These distributions provide free energy differences between Xe in various cage types in the same zeolite sample. Since the chemical potential for Xe in the different cage types are identical (all are at equilibrium with the same overhead Xe gas in the sample), the different $\langle n\rangle_{Xe}$ observed for the various cage types in the same sample directly provide differences in adsorption isotherms or ratios of Henry's law constants for the various cage types.

The chemical shifts for Xe_n in each cage type are shown in Table 1. We had tentatively assigned the observed two Xe_n progressions in Linde $4A$ to those Xe_n in the cavities of $Na_{12}A$ and $Ca_1Na_{10}A$. The $\langle n\rangle_{Xe}$ associated with the extra peaks assigned to $Ca_1Na_{10}A$ is clearly smaller than the $\langle n\rangle_{Xe}$ of the regular peaks observed in the pure $Na_{12}A$. On the other hand, upon low levels of Ca^{2+} ion exchange, we have produced a zeolite that upon calcination and thin-bed drying under vacuum in the usual manner, shows at least two types of cavity (plus a small amount of a third type), as indicated by Xe_n progressions that have distributions characteristic of different $\langle n\rangle_{Xe}$ values. The progression of peaks that are shifted to lower chemical shifts (the same as the secondary ones found in Linde $4A$) have a smaller value of $\langle n\rangle_{Xe}$ than the progression of Xe_n peaks that appear at the chemical shifts associated with $Na_{12}A$. The third type of cavity shows a progression of Xe_n peaks that appear at higher chemical shifts than those in pure $Na_{12}A$. At higher levels of Ca^{2+} ion exchange, a fourth type of cavity appears at even higher chemical shifts. The intensities of the latter are not large enough to permit accurate determination of $\langle n\rangle_{Xe}$, however. Values of $\langle n\rangle_{Xe}$ for Xe in equilibrium among several cavity types are shown in Table 2.

Briefly, the procedure used in obtaining Tables 1

Table 2
The experimental $\langle n\rangle_{Xe}$, Xe atoms per cage, obtained from the relative intensities of the Xe_n peaks assigned to $Ca_0Na_{12}A$, $Ca_1Na_{10}A$, Ca_2Na_8A, and Ca_3Na_6A cages in equilibrium with the same overhead gas in the same sample (inconclusive, for intensities too weak to provide a good value of $\langle n\rangle_{Xe}$)

	$Ca_0Na_{12}A$	$Ca_1Na_{10}A$	Ca_2Na_8A	Ca_3Na_6A
Linde $4A$, $\langle n\rangle_{Xe}^{overall} = 2.47$	3.50	1.85	Inconclusive	–
Linde $4A$, $\langle n\rangle_{Xe}^{overall} = 3.02$	3.60	2.49	Inconclusive	–
Linde $4A$, $\langle n\rangle_{Xe}^{overall} = 3.49$	4.07	2.84	Inconclusive	–
Linde $4A$, $\langle n\rangle_{Xe}^{overall} = 4.82$	5.32	4.07	Inconclusive	–
Linde $4A$ + 0.58 Ca/cage, $\langle n\rangle_{Xe}^{overall} = 2.50$	Inconclusive	2.34	2.65	Inconclusive

and 2 is as follows: As a starting point in the fitting, a hypergeometric distribution of Ca^{2+} ions among the cages was assumed. Knowing the average number of Ca^{2+} ions per cage from chemical analysis, making the assumption that there are 6 Ca sites and that a site can not be occupied by more than one Ca^{2+} ion, the strictly statistical hypergeometric model [22] provides the fraction of cages having zero, one, two, three,... Ca^{2+} ions. That is, for a stoichiometric formula $Ca_xNa_{12-2x}A$, the fraction of cages having exactly i Ca^{2+} ions is given by this model [17]:

$$H_i = \langle i \rangle^i (K - \langle i \rangle)^{(K-i)} K!/K^K i!(K-i)! \qquad (1)$$

This is the initial distribution of cages that starts the iterative fitting to experimental intensities. Initial values of the $\langle n \rangle_{Xe}$, that is the average number of Xe atoms per cage, are assumed for each cage type containing a specific number of Ca^{2+} ions. The $\langle n \rangle_{Xe}$ for cages containing Ca_1Na_{10} counterions, for example, is then used to generate an initial approximate distribution of Xe atoms among these cages, also using the hypergeometric model. It is known from experiments on Xe in pure $Na_{12}A$ that for $\langle n \rangle_{Xe} \leq 4.0$ the hypergeometric distribution gives a reasonably good description of the observed distribution. With this, the initial relative intensities of the peaks within the progression of peaks corresponding to $Ca_1Na_{10}A$ are generated. Thus, the relative intensities within the profile of one progression need not be individually adjusted in the fitting. In other words, the initial set of fractions of cages $Ca_0Na_{12}A$, $Ca_1Na_{10}A$, Ca_2Na_8A, Ca_3Na_6A,... are used to determine the relative total intensities of the progressions compared to each other, whilst the distribution of Xe among cages of a particular type determines the intensity profile for each type of cage. The Lorentzian–Gaussian line shapes at these chemical shifts for each Xe_n are then summed together to generate the expected total ^{129}Xe NMR spectrum in the zeolite. A few iterations provide the final set of values for the fractions of cages and the $\langle n \rangle_{Xe}$ for each type, shown in Table 2.

If the growing sets of peaks upon Ca^{2+} substitution could be assigned to Xe_n in $Ca_1Na_{10}A$, Ca_2Na_8A, and Ca_3Na_6A alpha cages, then denoting their respective average occupancy $\langle n \rangle_{Xe}$ as $\langle n \rangle_{Ca1}$, $\langle n \rangle_{Ca2}$, and $\langle n \rangle_{Ca3}$, and their respective Xe_n chemical shifts as δ_{Ca1}, δ_{Ca2}, δ_{Ca3}, the qualitative trends that are of interest in the results summarized in Tables 1 and 2 can be described as follows: For the comparative adsorption isotherms, the trends are,

$[\langle n \rangle_{Ca1} - \langle n \rangle_{Ca0}] < 0$ for all values of overall loading of Xe and

$[\langle n \rangle_{Ca2} - \langle n \rangle_{Ca1}] > 0$

In addition,

$[\langle n \rangle_{Ca3} - \langle n \rangle_{Ca0}] > 0$ for all Xe loadings

may be inferred from the work of Tsiao et al. [14]. For the chemical shifts of corresponding Xe_n, $n = 1$–5, the trends are,

$\delta_{Ca3} > \delta_{Ca2} > \delta_{Ca0} > \delta_{Ca1}$

$[\delta_{Ca1} - \delta_{Ca0}] < 0$ by about 3 − 5 ppm,

$[\delta_{Ca2} - \delta_{Ca0}] > 0$ by about 1 − 4 ppm,

and $[\delta_{Ca3} - \delta_{Ca0}] > 0$ by about 7 − 8 ppm.

We did not have a sample at high enough Xe loading to observe high intensities of Xe_6, Xe_7 and Xe_8 to carry out the same analysis for $n = 6$–8. Thus, the qualitative trends in the chemical shifts of the very crowded cages is presently unknown experimentally. We expect to be able to reproduce the above observed trends by GCMC simulations in $Ca_1Na_{10}A$, Ca_2Na_8A, Ca_3Na_6A compared to $Na_{12}A$.

In addition, we have made measurements of the adsorption isotherms and chemical shifts of Xe in fast exchange in Linde 5A, nominally Ca A, but with some Na. We have already seen, by the comparison between the ^{129}Xe NMR spectra of Xe sorbed in Na A and in Ca A, that the average chemical shift under fast Xe exchange (in the relatively open Ca A system) contains in it the information about the individual shifts associated with specific numbers of Xe atoms per cage (or Xe_n clusters) convoluted with the fractions of such cages in the zeolite appropriate to the average occupancy at a given temperature [17,23]. It was possible to understand qualitatively how the average chemical shift under fast exchange in the open pores of zeolite Ca A is determined by the individual properties of cages filled with n Xe atoms since we have directly observed the Xe_n distributions and chemical shifts in Na A [17]. A quanti-

tative interpretation will require that we know in what way the Xe chemical shift is affected by Ca^{2+} ions as opposed to Na^+ ions in the large cavities of the zeolite. With the new pairwise-additive intermolecular shielding functions we have constructed for rare gas–O and rare gas–Na^+, K^+, Ca^{2+} [24], we can carry out GCMC simulations in $Ca_xNa_{12-2x}A$, to see if we can reproduce the qualitative trends described above and the quantitative experimental results in Tables 1 and 2.

3. Grand canonical Monte Carlo simulations

The methods are described in our previous work on Xe in zeolites Na *A* and K *A* [18,19]. Here, we are concerned only with the part that is different from the previous work.

3.1. Polarization contributions to the potential energy

In our previous GCMC simulations [18,19,25], we did not include polarization explicitly, rather we used an effective Lennard–Jones potential for Xe–O and Xe–cation interactions to describe the entire interaction of a Xe atom with the zeolite. This was done to limit the number of parameters needed to describe the interaction, so as not to obscure the essential aspects of the distribution and Xe_n chemical shifts arising from the GCMC averaging with the flexibility afforded by a larger number of arbitrarily chosen parameters. The Lennard–Jones parameters used in our earlier work had been taken from the ones used by Woods and Rowlinson to describe the adsorption isotherm and isosteric heats of Xe in zeolite Na*Y* and Na*X* [26,27], with only one minor modification: The r_0 of the Xe–O potential was adjusted to prevent observation of visible Xe_9 peaks, in agreement with experiment. To preserve the agreement of the Rowlinson simulations with the Na*Y* adsorption isotherm, ε/k_B was paired with r_0 such as to preserve the volume of the bowl of the Xe–O potential. This was used without change for all Xe in Na*A* and K*A* simulations, which successfully reproduced not only the detailed distributions of Xe, but also the Xe_n chemical shifts and their temperature dependence in Na*A* (Xe with Ar and pure Xe), and also in K*A* [18,19,25]. For the interaction of Xe with these zeolite cages containing monovalent cations, separating out the polarization of Xe from the repulsive + dispersion contributions represented by the Lennard–Jones potential function would not significantly alter the agreement of the distributions and chemical shifts, provided that a suitable separation of the effective Xe–O and Xe–Na (or Xe–K) potentials into the polarization and the Lennard–Jones parts is carried out. The high symmetry of these cages helps in keeping the distributions and chemical shifts well-behaved. In contrast, partial replacement of Na^+ with a divalent cation leads to highly unsymmetrical cages and no effective Lennard–Jones-only description can compensate for the intrinsically greater polarization of Xe from Ca^{2+} ions compared to Na^+ ions, and for the successive changes in polarization that occur with two Ca^{2+} and three Ca^{2+} in the cage.

Thus, to interpret the experimental results for Xe_n in $Ca_xNa_{12-2x}A$ cages, we consider the polarization terms explicitly in this paper. The major problem associated with including polarization is the sharp increase in the number of parameters required to provide a description of the electrostatic potential. What is the true electrostatic potential inside a zeolite? This can be obtained experimentally from X-ray diffraction data. In principle, X-ray diffraction has always yielded the crystal electron density. The formalisms needed to analyze and parameterize this fundamental electrostatic quantity have been developed [28]. As a result, it is now feasible to obtain from X-ray data electrostatic properties such as the electrostatic potential and its derivatives (e.g., the electric field). The reliable estimation of the static electrostatic potential has been discussed by Spackman and Stewart [29,30]. The electrostatic potential for Na*A* has been determined by Spackman and Weber from Pluth and Smith's [21] refined single crystal X-ray data [31]. The most important result is the shape of the aluminosilicate framework. It is characterized by a large positive potential around each of the nuclei and looks very much like a model of the structure drawn with overlapping spheres. The important conclusion in the work by Spackman and Weber is that the electrostatic potential derived from X-ray diffraction data is nothing like the pictures of the electrostatic potential constructed by assuming

point charges at the atomic sites [32]. We should use actual X-ray diffraction data to obtain experimental electrostatic potentials for Ca_6A to compare with $Na_{12}A$, for silicalite to compare with various aluminated versions (ZSM-5), and various aluminated versions of faujasites (various NaY and NaX), in order to have a parameter-free description of the polarization energy of Xe in these zeolites. However, at this time, we require electrostatic potential information for zeolites which are disordered, i.e., with variable distributions of Ca^{2+} ions among the cages, but there is no X-ray diffraction data available from which to extract the electrostatic potential for each type of cage. Therefore, we are left with the simple option of using point charges just as other workers have done, thus including only the zeroth order term in the multipole expansion, for the purpose of calculating polarization contributions to adsorption energies in zeolites which are not cation-free.

It was concluded by Spackman and Weber that there is no way of reproducing the true electrostatic potential by using fixed partial point charges at the positions of the atoms and ions in the zeolite [31]. Parameterization of the polarization contribution to the potential energy by choosing the partial charges therefore can not be carried out on a physically meaningful basis without resorting to a fitting procedure of some type. The parameters that have been used previously by other workers have varied greatly and there is no objective way of choosing among them. The models which have been used are of the following types:

(1) In all-charged-atoms models, Si, Al, O and the cations are all assigned charges. (a) The zeolite may be assumed to be purely ionic so that the full charge of +4e for Si is assigned, +3e for Al, −2e for O atoms, and +1e for Na [32–34]. (b) Others assign partial charges on all atoms, including Si and Al. For example, the potential used to describe the aluminosilicate framework of anhydrous NaA and CaA zeolites for the purpose of predicting the structure and the infrared spectra has employed a Coulomb potential using charges on all atoms ($q_{Si} = +1.85e$, $q_{Al} = +1.27e$, $q_O = -1.03e$, $q_{Na} = +1e$, $q_{Ca} = +2e$), with various non-bonded interactions added, including neighbor TO–TO interactions and interactions between adjacent tetrahedra [35]. The all-charged-atoms model has been used by several authors. It is not uncommon to use different partial charge assignments for the same zeolite in doing simulations of different adsorbed molecules. For example for NaY, partial charges +0.80e for Na, −0.7e for O, +1.20e for Si and Al have been used when the sorbate is benzene [36], and changed to +1e for Na, and +1.15e for Si and Al when the sorbate is CH_4 [37,38].

(2) In the two-charge model, a charge is assumed for the cation and the charge of O is determined by electroneutrality, assuming Si and Al charges are zero (see references in Table 3). Variations include (a) full charges on the cations, all O atoms have the same partial charge determined by electroneutrality, (b) partial charges on the cations, all O atoms have the same partial charge determined by electroneutrality, and (c) full charges on cations ($q_{Na} = +1e$, $q_{Ca} = +2e$) and different partial charges on the O atoms depending on their location. For example, $q_O = -0.333e$ for oxygens in the 6-rings having a Na^+ ion in the center, and zero charge on all other O atoms, have been used [52].

A summary of charges used by various authors are shown in Table 3. Cohen de Lara et al. reported that the electric fields calculated at various positions inside the cavity are nearly the same for the purely ionic model ($q_{Si} = +4e$, $q_{Al} = +3e$, $q_O = -2e$, $q_{Na} = +1e$) [45] and the two-charge model, where the cation charge is taken to be the full charge and the partial charge on O ($q_O = -0.25e$) is found by electroneutrality. It has been found that full charge assignment on the cation ($q_{Na} = +1e$, $q_{Ca} = +2e$) gives too high isosteric heats of adsorption [52,58,56] compared to experimental data. Thus, to obtain isosteric heats closer to experiment while keeping the charges at zero on the Si and Al atoms, the charges on the cations have been adjusted to +0.66e for Na [53], or to different charges depending on the zeolite, +0.695e for Na in NaX, +0.376e for Na (and exactly twice this for Ca) in Ca_4Na_4A [54]. Bosacek and Dubsky concluded that +0.7e for Na fits NaY experiments best [56]. McCormick adopted this +0.7e charge for Na in GCMC simulations of Xe in a model cation-saturated NaA and found very high adsorption energies when the Lennard–Jones parameters used are from the most commonly adopted ones of Kiselev and Du [55]. With these various charge assignments, some of which are included in Table 3,

Table 3
The charge parameters in various models for polarization energies in zeolites

Model	Ref.	Zeolite	q_{Si}	q_{Al}	q_{Na}	q_{Ca}	q_O	q_O (other)
All-charge model								
Purely ionic	[32–34,39]	Na*A*, Ca_6A, Ca_4Na_4A, Na*Y*	+4e	+3e	+1e	+2e	−2e	Same
Full charge on cation, partial charges on others	[40]	Na*A*, Ca_6A	+1.85e	+1.27e	+1e	+2e	−1.03e	Same
	[41,42]	Na*A*	+3.5e	+3.5e	+1e		−2e	Same
	[37,38]	Na*Y*	+1.15e	+1.15e	+1e		−0.7e	Same
Partial charges on cation, one q_O	[36]	Na*Y*	+1.20e	+1.20e	+0.8e		−0.7e	Same
Partial charges on cation, variable q_O	[43]	Na*A*	+0.6081e	+0.6081e	+0.55e		−0.4431e	−0.4431e −0.4380e
	[44]	Ca_6A, Ca_4Na_4A	+0.6081e	+0.6081e	+0.55e	+1.10e	−0.4431e	−0.4431e −0.4380e
Two-charge model								
Full charge on cation, one q_O	[33,45,39,46–48]	Na*A*, Ca_6A, Ca_4Na_4A	0	0	+1e	+2e	−0.25e	Same
	[49,50]	Na*A*	0	0	+1e		−0.25e	Same
	[51]	$NaA_{Si/Al=2}$	0	0	+1e		−0.111e	Same
Full charge on cation, variable q_O	[52]	Na*A*, Ca_4Na_4A	0	0	+1e	+2e	−0.333e	0
Partial charge on cation one q_O	[53]	Na*X*	0	0	+0.66e		cb	Same
	[54]	Na*X*	0	0	+0.695e		cb	Same
	[54]	Ca_4Na_4A	0	0	+0.376e	+0.752e	cb	Same
	[55]	Na*A*	0	0	+0.7e		−0.175e	Same
	[56]	Na*Y*	0	0	+0.7e		−0.75e	Same
Variable charge cation one q_O	[57]	Na*Y*	0	0	+1eI,II +0.5667e for III		−0.15e	Same
	[57]	Na*X*	0	0	+1e for I,II +0.5667e for III		−0.20e	Same

the induction energy varied from about 20% [49] to about 60% [50] of the total calculated energy for Ar in Na*A*, for example. Similarly, various charge assignments lead to induction energies varying from about 20% [57] to 63% [53] for Xe in Na*X*. Such large variations preclude our adoption of one of the sets of charges used by previous authors.

One possible way of arriving at a set of partial charges for use in calculating the electrostatic potential is to use the Mulliken atomic populations from an SCF calculation of a fragment of the zeolite cage. The Mulliken charges correspond to a multicenter multipole expansion in which the centers are the atom and the multipoles of higher order than zero are neglected [59,60]. A better description could be obtained by representing the molecular charge distribution from the ab initio wave function by using Stone's multicenter multipole expansion [59,60], a distributed multipole analysis method which has been used successfully in the prediction of structure and dipole moments of van der Waals complexes [61]. Where others have considered, for example, Xe interacting with the CO_2 molecule by using a multicenter multipole expansion describing the charge distribution in CO_2 taken from an ab initio wave function, we would need instead a description of the charge distribution in a zeolite taken from an ab initio wave function of a zeolite supermolecule. The problem is the size of the cluster that will replace the whole real crystal. Vigne-Maeder and Auroux have instead attempted to represent the charge distribution in a zeolite by using as many as 1562 Si atoms which are either parts of monomers $Si(OH)_4$ or dimers $(HO)_3Si–O–Si(OH)_3$ [62]. The charge distribution was reconstructed from a sum of fragments by superposition and subtraction of parts in excess and then the distributed multipole analysis was carried out. This method does yield the correct relative ordering of heats of adsorption of a series of sorbate molecules, although quantitative agreement with experimental values were not obtained. We do not choose this method, but rather employ the simpler method of using Mulliken charges, thus completely neglecting the higher multipoles.

To find a set of Mulliken charges, we used the same zeolite fragments that were used in the calculations of rare gas atom shielding in a zeolite cage [24]. This leads to different charges on Na depending on the type of Na site, as it should, but does not converge to a consistent set of partial charges upon systematically increasing fragment size and basis set size. A plot of the Mulliken charges on the Na atom in one particular zeolite fragment (the 6-ring $[Si_3Al_3O_6(OH)_{12}]Na_3$) against basis set size used is shown in Fig. 2. Here, only the Na^+ ion, in the center of the 6-ring coordinated to the oxygens of the framework, is being examined. The other two Na^+ ions in the fragment are located in their positions in site I of the zeolite, but only partially coordinated to oxygen atoms due to the limited size of the fragment. The Pople basis sets yields positive charges $q_{Na} = +(0.631–0.701)e$, which are lower than those obtained from Huzinaga [63] basis sets, $[q_{Na} = +(0.910–1.00)e]$, as a general trend. Using the effective core potential (ECP + DZ) leads to $q_{Na} = +0.698e$. Including polarization functions gives smaller charge separations. The charge on the coordinated Na depends on the type of site, and the charge on the O atoms varies with its distance from the cation. We found that for Si–Al ratio of 1 in the

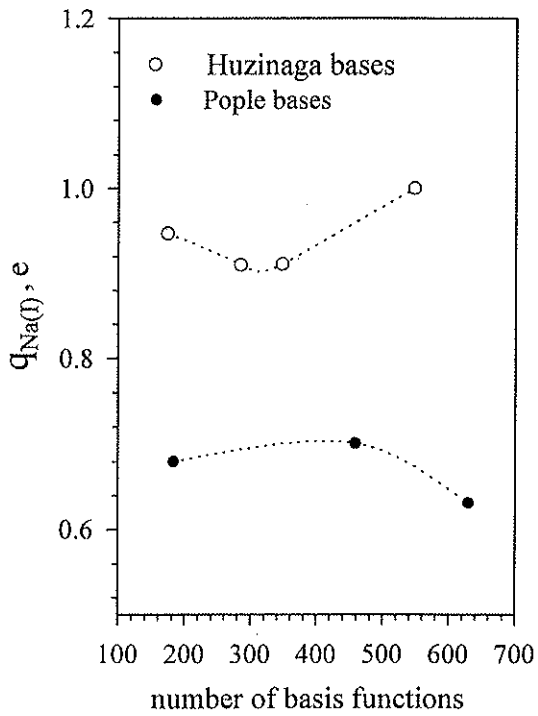

Fig. 2. Charges on the Na in the center of the ring in the fragment $[Si_3Al_3O_6(OH)_{12}]$ Na_3, obtained from a Mulliken population analysis, using various basis sets. The Pople basis sets used were STO-3G (183), 6-311G (459), 6-311G** (630), and the Huzinaga basis sets used were MINI (174), VDZ (285), DZ (348), DZVP (548).

zeolite fragment, the charge difference between Si and Al is of the order of 0.44e to 0.47e at the 6-311G basis set, and 0.25e to 0.30e at 6-311G**. The latter is the same as the 0.26e charge difference that was used by Herrero for all Si/Al ratios in the simulations of the Si and Al distribution in *A* type zeolites [64]. If we adopt the 6-311G** basis set, we find partial charges +1.8e for Si, +1.55e for Al, −1.0e for O atoms. At the same time we find +0.573e, +0.631e and +0.800e respectively for the unique Na(III) inside the alpha cage, the Na(I) in the 6-rings and the Na(II) in the 8-ring windows of Na*A*. Where the same family of basis sets are used for both Ca and Na atoms, Mulliken population analysis leads to the Ca/Na charge ratio in the same zeolite cage fragments. For the 6-ring fragment, our calculations show that this is close to 2.0 and can vary from 1.57 to 2.4, depending on the basis set used.

On the basis of SCF calculations in zeolite fragments having 20–52 atoms using the 6-311G** basis set (the same fragments used in Ref. [24] for ab initio calculations of the chemical shifts of a rare gas atom in the presence of a zeolite), we arrived at a set of Mulliken atomic charges, given in Table 4. Some justification of our choice of this set is afforded by the following: The 0.26e difference between Si and Al is the same as that which has been used by Herrero in simulations of the T (Si or Al) atom distributions in *A*-type zeolites [64]. The average charge on Na is close to the average of $q_{Na(I)} = +0.612e$ and $q_{Na(II)} = +0.66e$ which has been found to reproduce the experimental far infrared spectrum of Na*A* involving the Na(I) and Na(II) vibrational modes [66]. The charges adopted here are consistent with the finding by Cohen de Lara that $q_{Na} \approx +(0.6–0.7)e$ and the sum $(q_{Na} + q_{Si} + q_{Al}) \approx 4.0e$, the so-called ionicity of the zeolite, give the best agreement with the vibrational frequency shift observed in H_2 molecules adsorbed in Na*A* zeolite [67]. In Table 4, we have +0.63e and +4.01e for these quantities, respectively.

The polarization contribution to the potential energy of a Xe atom in the zeolite is calculated using this set of partial charges. For each zeolite structure used, the electric field was calculated at a fine grid of points ($60 \times 60 \times 60$, 0.2 Å between points) and saved. During the GCMC simulations, these values

Table 4
The partial charges used to calculate the polarization energies for Xe atoms in $Ca_xNa_{12-2x}A$ zeolite cages (this work), and also Na*Y* and Na*X* zeolites (Ref. [65]), derived from Mulliken charges resulting from calculations on several zeolite fragments having 20–52 atoms, using 6-311G** basis sets

	Partial charge
Si	+1.82e
Al	+1.56e
O	−1.025e
Na	+0.63e
Ca	+1.26e

are retrieved via table look-up with interpolation for the specific location of a Xe atom. The polarization energy is added to the pairwise-additive contributions from the Lennard–Jones potential which represents the repulsive and dispersion parts of the total potential energy of interaction between each Xe atom and the zeolite. The Lennard–Jones parameters given in Table 5 were found by following the suggestion of Woods and Rowlinson: Using a starting set of r_0 and ε for Xe–O and Xe–cation, a single parameter β was used to scale the attractive part of the Lennard–Jones function, thereby, only one parameter is adjusted in the partitioning of polarization and Lennard–Jones during the fitting to some properties of the zeolite.

$$V^{LJ} = Ar^{-12} - \beta Br^{-6} \tag{2}$$

Once the partial charges were adopted from the Mulliken atomic charges, β was adjusted to provide overall agreement in Xe adsorption isotherms and maximum Xe occupancies of several zeolites together (*A*, faujasites *X* and *Y*) using the same Lennard–Jones parameters for Xe–O and Xe–Na interactions for all.

With the parameters given in Tables 4 and 5, the partitioning of polarization vs. Lennard–Jones contributions to the configuration energy for $\langle n \rangle_{Xe} \sim 1.0$ varied from $U_{ind}/U_{total} = 5\%$ in Na*Y* (48 Na^+ ions) to 39% in Na*X* (88 Na^+ ions). For the $Ca_xNa_{12-2x}A$ series, it varied from 20% in $Ca_0Na_{12}A$ to 4% in $Ca_1Na_{10}A$, to 31% in Ca_2Na_8A, to 55% in Ca_3Na_6A. For a given zeolite framework, one might expect the fraction of the total energy coming from polarization to increase with increasing number of divalent cations, however, the symmetry of the ar-

Table 5
The Lennard–Jones parameters used in the GCMC simulations which separately include polarization energy, used in this work and used also in NaY and NaX zeolites and silicalite (Ref. [65])

	Set I effective Lennard–Jones, [18] no separate polarization energy $\beta = 1.00$		Set II Lennard–Jones, [this work] added to separate polarization energy $\beta = 0.88$	
	r_0, Å	ε/k_B, K	r_0, Å	ε/k_B, K
Xe–O	3.37	217	3.443	168
Xe–Na	3.676	39.08	3.755	30.26
Xe–Ca	4.2	45	4.29	34.85

These are related to previously used parameters (Refs. [18,19,25]) by $\beta = 0.88$ in Eq. (2).

rangement of ions affects this fraction to a large extent. For example, in going from $Ca_0Na_{12}A$ to $Ca_1Na_{10}A$, the loss of the Na(III) situated off-center inside the alpha cage actually leads to a smaller polarization energy in the Ca_1 cages compared to the Ca_0 cages.

3.2. Coordinates of the cations

For the GCMC simulation of Xe in zeolite NaA substituted with Ca^{2+} ions, $Ca_xNa_{12-2x}A$, the coordinates of the zeolite framework atoms and cations in the simulation box were chosen as follows. Pluth and Smith's single crystal refinements of coordinates for zeolite NaA were used for $Na_{12}A$ [21]. The positions of the Ca^{2+} ions in the $Ca_1Na_{10}A$, Ca_2Na_8A, and Ca_3Na_6A zeolites are not known. Pluth and Smith have reported the X-ray structure of nearly pure Ca_6A [68]. Would the Ca^{2+} ions be located more into the alpha cages as nearly all the ions in Ca_6A of Pluth and Smith's structure, or would they be located more like the structure for dehydrated Ca_5Na_2A reported by Adams and Haselden, based on neutron scattering [69]? The latter suggests that all Ca^{2+} ions are located almost in the centers of the 6-ring sites, only a bit inside the beta cage, and that the 6-rings are severely distorted whenever they are coordinated to Ca^{2+} ions. We considered each of these two X-ray structures as starting points for choosing coordinates of Ca^{2+} ions in the $Ca_1Na_{10}A$, Ca_2Na_8A, and Ca_3Na_6A cages for our simulation box.

We start with the well established NaA structure by Pluth and Smith [21] for the locations of the Na^+ ions and the framework atoms. In choosing the coordinates of the cations, the first point that has to be established is: Which two Na^+ ion sites are replaced by a Ca^{2+} ion? Since the progressions of individual Xe_n peaks are preserved in our NMR spectra, this must mean that the Ca^{2+} substitutions removed a negligible number of Na(II) ions. These site (II) ions are located in the plane of the 8-ring windows of the alpha cage. Removal of these ions would have opened up the alpha cages and permitted the Xe atoms to average their chemical shifts over 2 or more cages. Since there was no experimental evidence of this, then in all our simulation boxes in this work we have kept the Na(II) positions occupied. If no site (II) Na^+ ions have been replaced, then the Ca^{2+} ion must have replaced two Na^+ ions from the sites Na(III) and Na(I). The (III) site is inside the alpha cage, off-center, coordinated to the oxygens of a 4-ring. We assume that one Na(III) and one Na(I) are replaced by the first Ca^{2+} ion to go in. We reported experimental evidence for this in the Xe_n chemical shifts [20], which we expect to be quantitatively verified by the GCMC simulations. Furthermore, calculations of crystal energies using very simple potential models to discover the site selectivity of divalent cations in NaA have suggested that Na(III) has the least stabilization energy [41] and that the Na^+ ion in site III and one on either site I or II are exchanged [42]. We found that the precise location of the first Ca^{2+} ion in $Ca_1Na_{10}A$ is not a sensitive parameter in the simulations. We tried placing this first Ca^{2+} ion more inside the alpha cage according to the Pluth and Smith coordinates for Ca_6A and also a bit more into the beta cage according to the Adams and Haselden structure for Ca_5Na_2A. The Coulomb energy calculated using full charges on the cations only, for one alpha cage surrounded by 26 alpha cages, is lower if we use the

Pluth and Smith coordinates. Finally, we used the Pluth and Smith coordinates for the Ca^{2+} ion in the Ca_1Na_{10} *A* cages of our simulation box.

We considered several Ca^{2+} ion arrangements for the Ca_2Na_8 *A* cages. We calculated the Coulomb energy for each arrangement replicated in an alpha cage surrounded by 26 alpha cages. The Ca_2Na_8 *A* cages in the actual zeolite are expected to be a distribution among various arrangements of 2 Ca^{2+} ions, not only the lowest energy arrangement. Thus, as a typical Ca_2Na_8 *A* cage, we chose one of the low energy arrangements, though not specifically the arrangement with the lowest Coulomb energy. For the Ca_3Na_6 *A* cage there are a large number of possibilities and the GCMC results are more sensitive to the specific arrangement of three Ca^{2+} ions in Ca_3Na_6 *A* than to the arrangement of two Ca^{2+} ions in Ca_2Na_8 *A*, especially for the highly loaded cages. Since we have no experimental observations on Xe_7 and Xe_8 in these cages, we are unable to adequately test the arrangements of 3 Ca^{2+} ions. We have chosen to represent a typical Ca_3Na_6 *A* cage by one of the lower energy arrangements, not specifically the lowest energy one. We used the Adams and Haselden coordinates [69] for Ca_5Na_2 *A* to represent our 'Ca *A*' sample (dehydrated Linde 5*A* manufactured by Union Carbide), which is the same commercially available sample used by Adams and Haselden

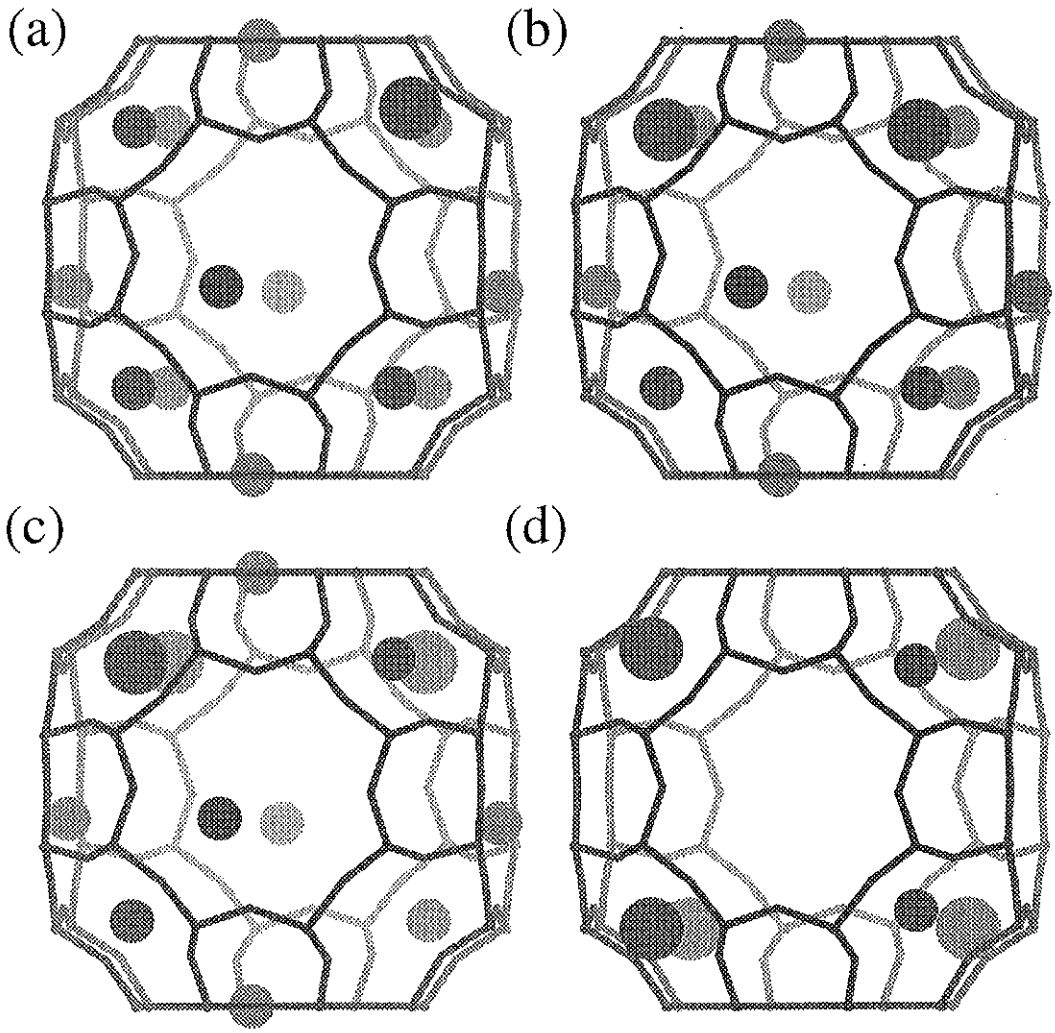

Fig. 3. Cation positions used in the GCMC simulations to represent the typical zeolite cages of Ca_1Na_{10} *A*, Ca_2Na_8 *A*, Ca_3Na_6 *A* and Ca_5Na_2 *A*. Lattice parameter = 24.555 Å was used for all types of cages. The framework atoms and Na^+ ions were located according to the unique coordinates from Pluth and Smith's refinement of the Na *A* structure [21], and the Ca^{2+} ions were located according to Pluth and Smith's structure for Ca_6A [68].

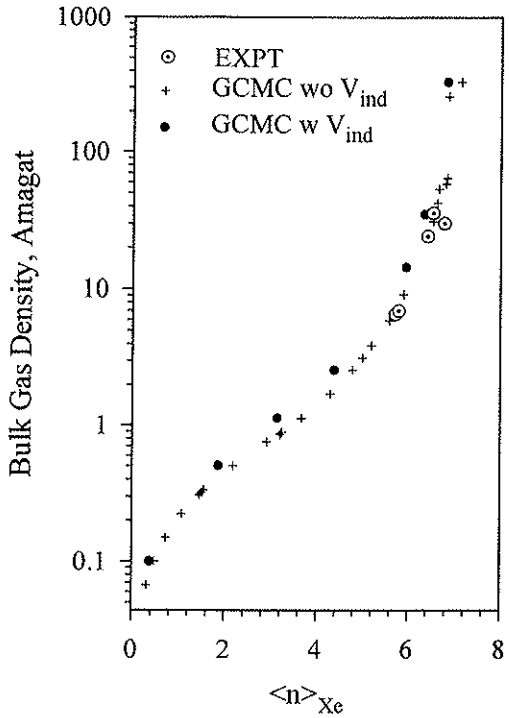

Fig. 4. Adsorption isotherm of Xe in Na A from GCMC simulations with and without explicit polarization terms, compared with experimental data (⊙) obtained from the gas density derived from the chemical shift of the gas peak at high loading [17].

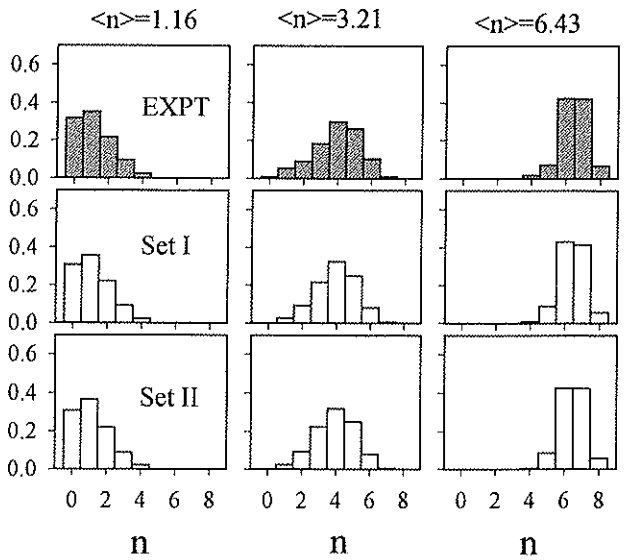

Fig. 5. Comparison of the distributions of Xe atoms among the alpha cages of Na A. The bar graphs provide the fractions of alpha cages containing n Xe atoms in various samples having the overall $\langle n \rangle_{Xe}$ shown at the top, from experiment [18] are compared with those obtained from GCMC simulations using the original effective Lennard–Jones parameter set I, that is, using $\beta = 1.0$ just as was used in Ref. [18], and with GCMC simulations in this work, using a separate polarization contribution and $\beta = 0.88$, that is, Lennard–Jones parameters set II, given in Table 5.

for their structure determination. In Fig. 3 are the set of cation coordinates we used for the typical alpha cages in the simulations of Xe_n in $Ca_1Na_{10}A$, Ca_2Na_8A, and Ca_3Na_6A cages and in the open Ca_5Na_2A cages.

4. Results

We have used the parameters given in Tables 4 and 5 in all simulations reported here. To see how including polarization has affected the characteristics of Xe in the zeolite Na A ($Ca_0Na_{12}A$) we show the results of GCMC simulations in Figs. 4–7. The previously reported GCMC results used no separate polarization terms, that is, used parameter set I in Table 5. The adsorption isotherms in Fig. 4 obtained from GCMC simulations with and without explicit

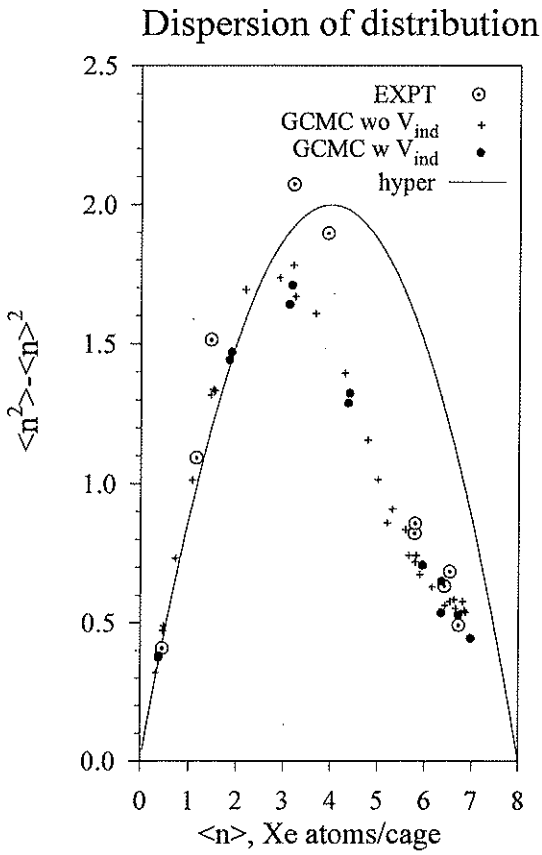

Fig. 6. Dispersion of the distribution of Xe atoms among the alpha cages of Na A, $[\langle n^2 \rangle_{Xe} - \langle n \rangle^2_{Xe}]$, obtained from experiment and from GCMC simulations with and without explicit polarization terms, compared with that obtained from assuming a hypergeometric distribution.

polarization terms are very similar and both compare well with experimental isotherms at high loading. The distributions in Figs. 5 and 6, from simulations including polarization using the set II parameters in Table 5, are comparable to the ones that were published previously [18]. In Fig. 7, the GCMC results for the Xe_n chemical shifts using Set II are just as close to the room temperature experimental values as the previous results. The temperature dependence of the Xe_n chemical shifts were reproduced very well by parameter set I, without separate polarization terms (published previously) [18] and are just as well described by set II, as shown in Fig. 7. Nevertheless, we do not consider set II as an optimized set of Lennard–Jones parameters (for Si/Al = 1.0) for partitioning the Xe in zeolite energy into $V_{\text{induction}}$ and $V_{(\text{repulsive}+\text{dispersion})}$. Rather it is a parameter set used to investigate the effects of polarization, obtained by adjusting a single parameter ($\beta = 0.88$), the factor that reduces the attractive part of the original Lennard–Jones. It achieves a reasonable description of the Xe_n chemical shifts at room temperature, as a

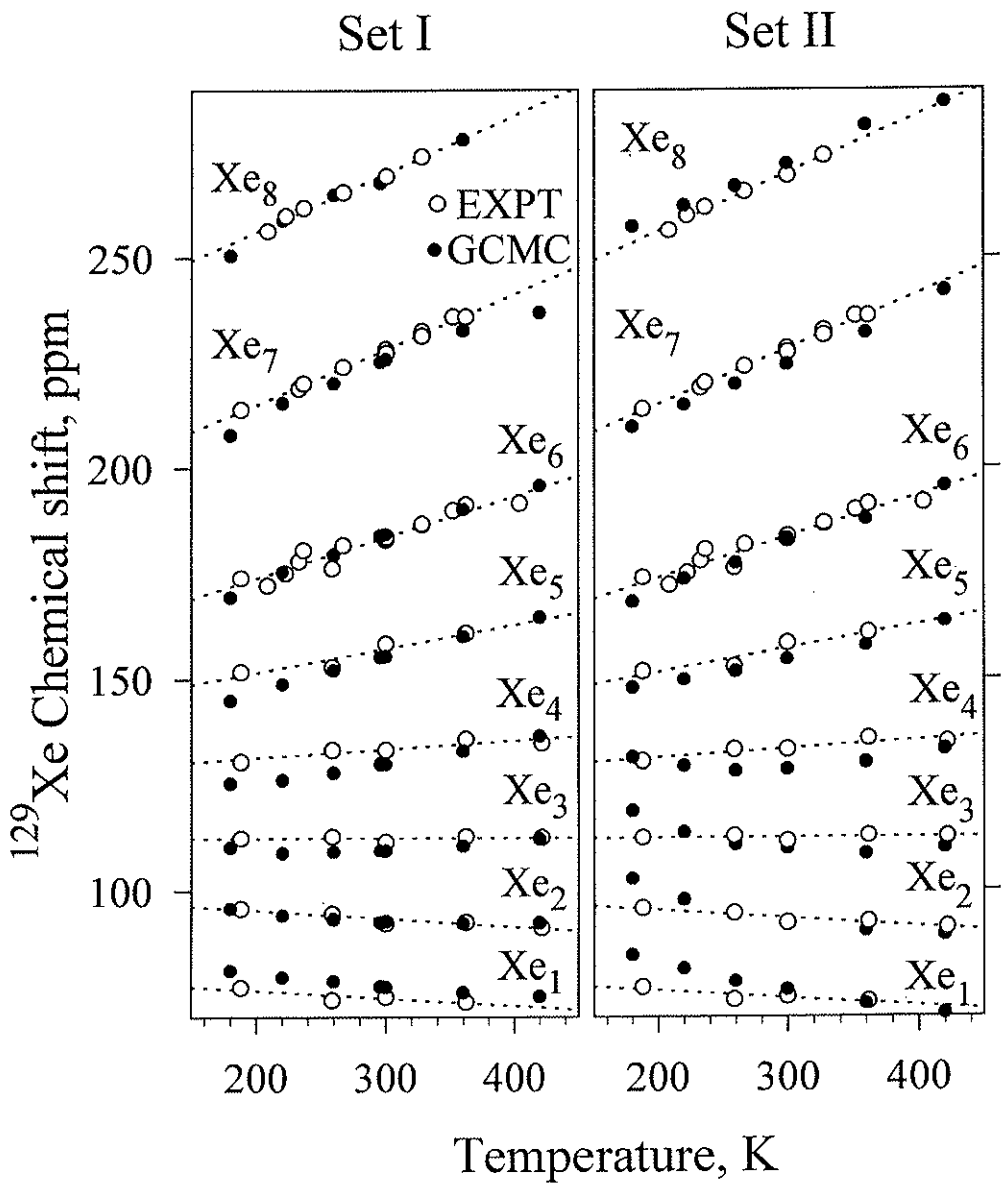

Fig. 7. Comparison of the temperature dependence of the ^{129}Xe chemical shifts of Xe_n in Na A obtained from GCMC simulations (a) Using a separate polarization contribution and $\beta = 0.88$, that is, Lennard–Jones parameters set II, given in Table 5 [this work] and (b) Using $\beta = 1.0$, that is, the original effective Lennard–Jones parameter set I, reported in Ref. [18].

function of temperature, and the Xe adsorption isotherm at high loadings (i.e., the maximum occupancy of the alpha cages of Na A). Therefore, we view parameter set II as a useful starting point for GCMC simulations including polarization energy for Si/Al = 1. As will be shown below, it will suffice for the purposes of examining the qualitative trends found experimentally in Ca-exchanged Na A.

The results of the GCMC simulations in the cages $Ca_0Na_{12}A$, $Ca_1Na_{10}A$, Ca_2Na_8A, and Ca_3Na_6A are shown in Figs. 8 and 9. The Xe_n chemical shifts at 300 K are shown in Fig. 8. Since our main interest here is the change upon substitution of Ca^{2+} ions for Na^+ ions, we show only the difference between the all-Na cages (normal Na A) and the three Ca-substituted cages. The qualitative trends in the Xe_n chemical shifts are indeed reproduced. The first Ca^{2+} substitution causes the Xe_n chemical shifts to uniformly decrease relative to the all-Na cage The next Ca substitution causes a substantial increase in the chemical shifts for all Xe_n. The third Ca^{2+} ion causes a further increase. In Fig. 9, we see that the

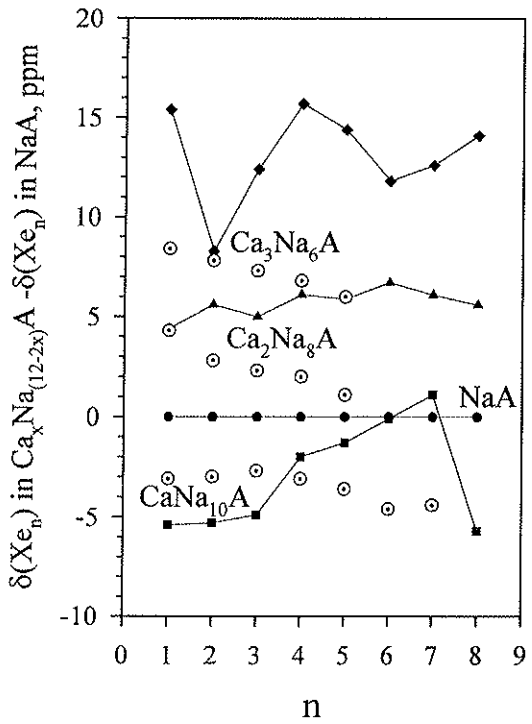

Fig. 8. The ^{129}Xe chemical shift change upon substitution of 1, 2, 3, Ca^{2+} ions into the zeolite A cage are obtained for the Xe_n peaks from GCMC simulations in $Ca_0Na_{12}A$, $Ca_1Na_{10}A$, Ca_2Na_8A, and Ca_3Na_6A and compared with experiment (⊙) as observed under MAS NMR [20].

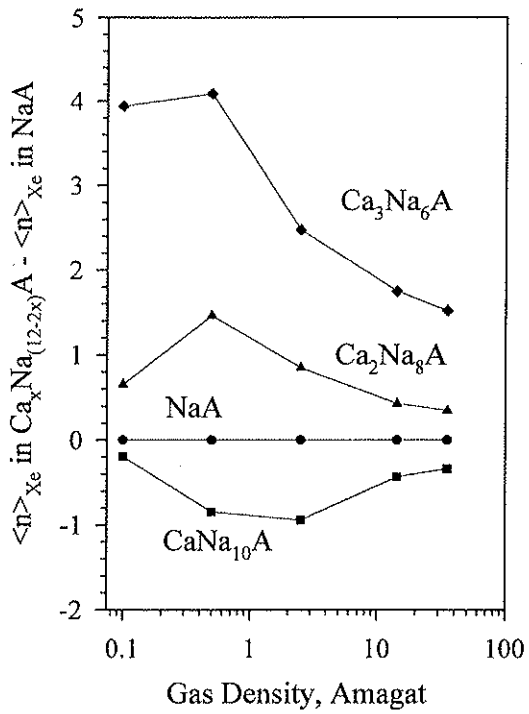

Fig. 9. The changes in the adsorption isotherm upon substitution of 1, 2, 3, Ca^{2+} ions into the zeolite A cage obtained from GCMC simulations at the same Xe chemical potential in $Ca_0Na_{12}A$, $Ca_1Na_{10}A$, Ca_2Na_8A, and Ca_3Na_6A cages. 1 amagat = 2.867×10^{25} molecules m^{-3} is the number density of an ideal gas under standard conditions of 1 atm and 0°C.

adsorption isotherms of the four types of cages are different from each other. That the first Ca^{2+} substitution causes a decrease in the value of $\langle n\rangle_{Xe}$ is very clearly seen in the experimental spectra. Fig. 9 shows that the GCMC simulations reproduce this. There is, of course, a monotonic increase in $\langle n\rangle_{Xe}$ with increasing overhead gas density, as we have observed in simulations of all-Na zeolite A, but what is shown in Fig. 9 are only the differences between the all-Na-cages and the cages with 1, 2, or 3 Ca^{2+} ions. The qualitative trends in these adsorption isotherms agree with those observed experimentally.

We show the results for Ca_5Na_2A, in Figs. 10 and 11. The GCMC results in Fig. 10 are in reasonable agreement with the adsorption isotherm that we reported previously in Ref. [23] for Ca A (Linde 5A), and with the adsorption isotherm reported by Tsiao et al. [14] at 300 K for $x = 5.9$ (and for $x = 4.9$ it is very nearly the same). The average ^{129}Xe chemical shifts under free exchange in Ca A shown in Fig. 11 from our previously published experiments in Ref.

[23] and the chemical shift data of Tsiao et al. [14] are reasonably reproduced by the present GCMC simulations in Ca_5Na_2A, although the simulations show a bit more curvature in the dependence of the average Xe chemical shifts on the overall $\langle n \rangle_{Xe}$ compared to experiments.

The most important result of the GCMC simulations carried out here is that the qualitative trends described in Section 2 are reproduced, as soon as polarization is included in the potential energy with reasonable pairwise-additive Lennard–Jones functions to make up the total adsorption energy. The specific choices for partial charges used for the framework atoms and cations, and the ratio of Ca/Na partial charges, change the calculated magnitudes of the shifts and $\langle n \rangle_{Xe}$, of course, but the observed qualitative trends are found in GCMC simulations using any reasonable set of partial charges adopted from SCF calculations in the zeolite fragments using any basis set, or using any of the partial charges previously used by other workers. That is, all give $\delta_{Ca1} < \delta_{Ca0}$ and all give δ increasing with increasing number of Ca substitutions: $\delta_{Ca3} > \delta_{Ca2} > \delta_{Ca1}$. This implies that the assignment of the progression of peaks to the cage types we have assumed is probably correct. Similarly, the exact choice of Ca coordinates in each cage type from among the Pluth–Smith or Adams–Haselden coordinates in Ca_6A or Ca_5Na_2A did not affect the qualitative trends. The change in the Xe_6, Xe_7, and Xe_8 chemical shifts in the crowded cages was, not unexpectedly, very sensitive to the choice of the Ca positions in Ca_3Na_6A. However, since we did not observe these changes experimentally, we could not test which of the many likely arrangements of 3 Ca^{2+} ions is in better agreement with experiment.

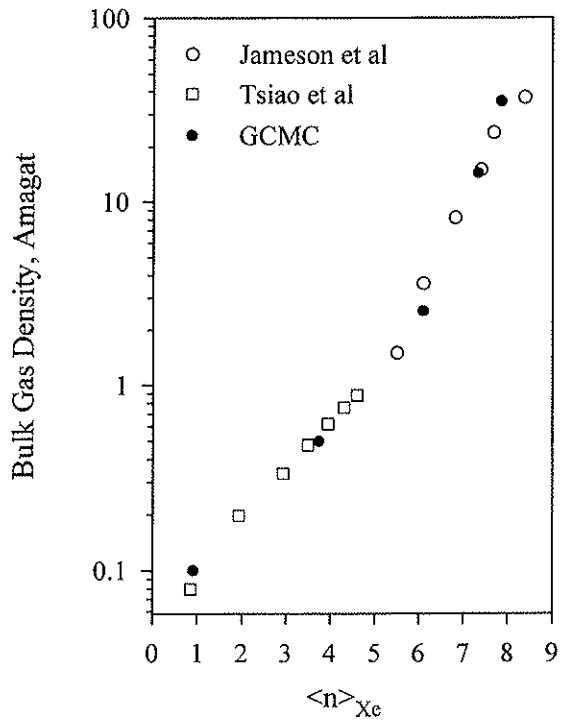

Fig. 10. The adsorption isotherm obtained from GCMC simulations (●) in Ca_5Na_2A cages are compared with the experimental adsorption isotherms obtained from NMR measurements (○) in our previous work, Ref. [23] and from conventional adsorption isotherm measurements (□) reported by Tsiao et al. in Ref. [14].

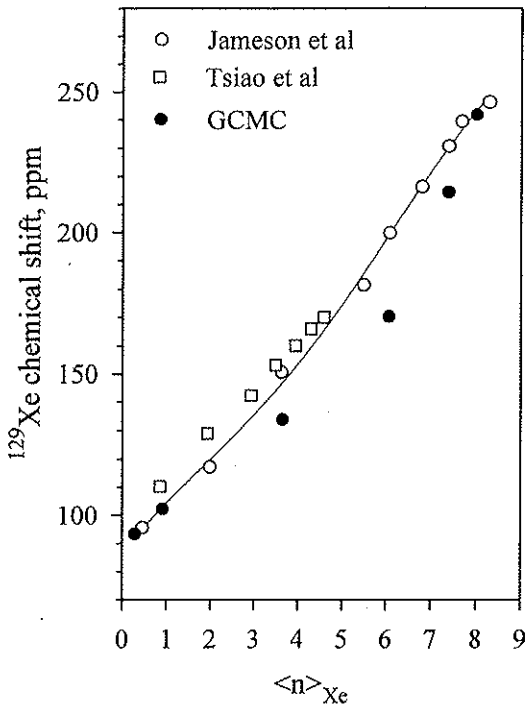

Fig. 11. The average ^{129}Xe chemical shifts observed (○) under fast exchange in Linde 5A in our previous work, (Ref. [23]) and that observed (□) in $Ca_{4.9}Na_{2.2}A$ by Tsiao et al. (Ref. [14]) are compared with the results of our GCMC simulations (●) in Ca_5Na_2A cages.

5. Discussion

5.1. The adsorption isotherms

A very clear experimental trend is $\langle n \rangle_{Ca0} > \langle n \rangle_{Ca1}$, which we correctly reproduce in the simula-

tions using any of the sets of parameters from the literature or our own set. This is easily understood if we believe that Na(III) is absent in $Ca_1Na_{10}A$ cages and provided induction terms are included. The weaker adsorption of Xe in $Ca_1Na_{10}A$ cages compared to $Ca_0Na_{12}A$ cages is largely due to the loss of Na(III). The experimental estimates for $\langle n\rangle_{Ca3}$ and $\langle n\rangle_{Ca2}$ are poor. A reliable estimate of $\langle n\rangle_{Ca3}$ requires good relative intensities of the members of the Xe_n progression assigned to Ca_3Na_6A cages. Since the peaks are small, we could not determine reliable estimates of $\langle n\rangle_{Ca3}$ very well. The situation for $\langle n\rangle_{Ca2}$ is somewhat better. Still there are relatively large error bars because estimates required deconvolution of overlapping peaks. Nevertheless, the trends are what we are interested in, and the GCMC results in Fig. 9 clearly produce the qualitative experimental trend $\langle n\rangle_{Ca3} > \langle n\rangle_{Ca2} > \langle n\rangle_{Ca0} > \langle n\rangle_{Ca1}$ in the same sample in equilibrium with the same gas. We find that, using any of the charges adopted by previous workers, the trend $\langle n\rangle_{Ca3} > \langle n\rangle_{Ca2} > \langle n\rangle_{Ca1}$ is preserved. And, the trend $\langle n\rangle_{Ca0} > \langle n\rangle_{Ca1}$ is found in every instance, provided only that Na(III) is replaced when the first Ca^{2+} ion substitutes for two Na^+ ions. The relative order $\langle n > _{Ca2} > \langle n\rangle_{Ca0}$ is not always the same for different partial charge assignments, however. Fig. 9 is also consistent with the adsorption isotherms in $Ca_xNa_{12-2x}A$ with variable x, previously reported by Tsiao et al. [14]. They found that at the same temperature, the adsorption isotherms exhibit an increase in adsorption with increasing x in the range $x = 1.2$–4.9. The qualitative trend of increased adsorption upon increase in Al (and cation) content observed in faujasites has also been reproduced in GCMC simulations provided that polarization terms are included [65].

5.2. The ^{129}Xe chemical shifts of Xe_n in Ca-substituted alpha cages

The qualitative trends observed in the changes in the Xe_n chemical shifts upon Ca-ion substitution, $\delta_{Ca3} > \delta_{Ca2} > \delta_{Ca0} > \delta_{Ca1}$ for each Xe_n, $n = 1$–5 are reproduced by the GCMC simulations in Fig. 8. Other assignments of partial charges give the same qualitative trends $\delta_{Ca0} > \delta_{Ca1}$ and $\delta_{Ca3} > \delta_{Ca2} > \delta_{Ca1}$, with the relative order δ_{Ca2} vs. δ_{Ca0} varying more with charge assignments. Although the experimental Xe_n peaks assigned to Ca_3Na_6A cages have small intensities, the chemical shifts should still be reliable, unlike $\langle n\rangle_{Ca3}$. Including polarization contributions to the energy produces these trends, whereas effective Lennard–Jones only V(Xe–O) potentials do not. Removal of the Na(III) during the substitution of the first Ca^{2+} ion is essential to the GCMC simulation finding that $\delta_{Ca0} > \delta_{Ca1}$ for Xe_n, $n = 1$–5. The contributions to the shielding from the Xe–Na shielding function for the Na(III) are larger than those from the other Na sites since site III is well into the alpha cage, leading to $\delta_{Ca0} > \delta_{Ca1}$ for the larger clusters Xe_4–Xe_6 even when all-Lennard–Jones effective Xe–zeolite potentials are used. However, the effect becomes generally true for all size clusters when Xe polarization terms are included explicitly. Thus, the experimental finding that $\delta_{Ca0} > \delta_{Ca1}$ for Xe_n, $n = 1$–5 can only be explained if Xe polarization is included explicitly. Furthermore, without the polarization terms, the qualitative trend $\delta_{Ca3} > \delta_{Ca2} > \delta_{Ca1}$ could not be obtained while maintaining reasonable agreement with adsorption isotherms for Ca_5Na_2A, by adjusting the effective Xe–Ca Lennard–Jones parameters. Thus, including polarization was absolutely necessary for the interpretation of the ^{129}Xe NMR experiments in Ca-exchanged NaA zeolite. A more general conclusion is that the effects of divalent-for-univalent ion exchange on Xe chemical shifts in zeolites are intimately connected with polarization of the Xe.

The dependence of the average Xe chemical shift under fast exchange in $Ca_xNa_{12-2x}A$ has been studied by Tsiao et al. for variable x, where x indicates the average Ca content [14]. At a sufficiently high value of x, the loss of Na(II) ions opens up enough windows that Xe is in fast exchange among numerous interconnected cages. In all their samples, the Xe is in fast exchange among the cages. The dependence of the average Xe chemical shift on the loading of Xe in the sample of zeolite with the highest Ca content from Ref. [14] is the one shown in Fig. 11, where it is compared to our data previously reported for CaA [23]. At other values of average Ca content, the experimental dependence of the average Xe chemical shift on $\langle n\rangle_{Xe}$ has a similar shape. The GCMC simulations in Ca_5Na_2A reproduces the experimental trend, although quantitative agreement is

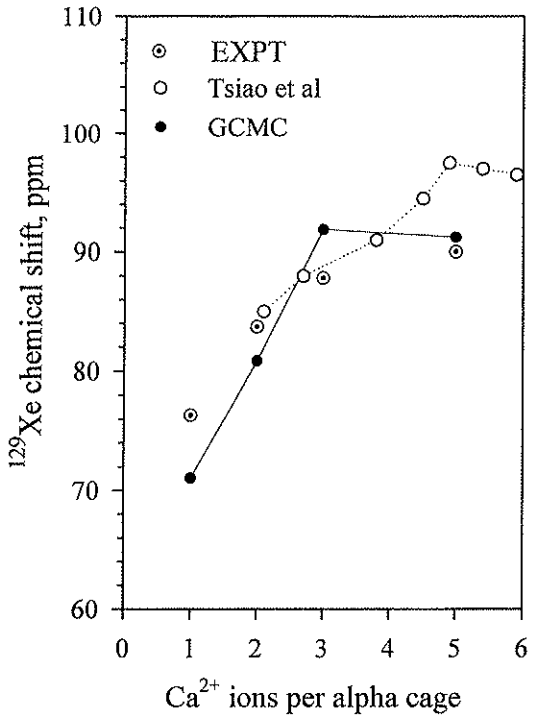

Fig. 12. The average ^{129}Xe chemical shifts observed under fast exchange in the zero-Xe loading limit (○) has a dependence on the Ca content in $Ca_xNa_{12-2x}A$ zeolite, observed by Tsiao et al. [14]. This is effectively the chemical shift of a single Xe atom in an open $Ca_xNa_{12-2x}A$ zeolite framework. These are compared with the ^{129}Xe chemical shifts of a single Xe atom in the cages $Ca_0Na_{12}A$, $Ca_1Na_{10}A$, Ca_2Na_8A, and Ca_3Na_6A from GCMC simulations (●), and the observed chemical shifts of the peak assigned to the Xe_1 signal in these cages, (⊙) as observed under MAS NMR [20].

only fair. At the limit of zero-Xe loading, Tsiao et al. provide the dependence of the Xe chemical shift on x. On their data, shown in Fig. 12, we have superimposed our experimental data for Xe_1 and the GCMC results for Xe_1 in the $Ca_0Na_{12}A$, $Ca_1Na_{10}A$, Ca_2Na_8A, and Ca_3Na_6A cages. We also show the GCMC results at the zero loading limit in Ca_5Na_2A cages. We see that we reproduce the trends observed experimentally rather well. (The qualitative trend of an initial increase for Xe_1 in going from $Ca_1Na_{10}A$, to Ca_2Na_8A, to Ca_3Na_6A cages, but not the plateau, is found in any of the charge parametrizations we tried). The chemical shifts of the various Xe_1 peaks in the four types of cages obtained upon Ca^{2+} replacement of Na^+ in NaA [20] are in excellent agreement with the observed dependence on the Na/Ca ratio of the ^{129}Xe chemical shift at the zero-loading limit in the open $Ca_xNa_{12-2x}A$ zeolite framework (at higher Ca exchange levels) [14]. There is a linear increase and then a leveling off. It should be noted that Dybowski's low loading chemical shifts involved a distribution of x values in $Ca_xNa_{12-2x}A$ giving rise to an average Ca content, and the abscissa value of x in Fig. 12 is their average Ca content for each sample shown. On the other hand, the numbers from our GCMC simulations are for Xe_1 in alpha cages having a constant value of $x = 1$, 2, 3 or 5, and our experimental data are (as assigned) for a single Xe atom in alpha cages having a constant value of $x = 1$, 2, or 3 Ca^{2+} ions.

In Figs. 13 and 14, we show simulated NMR spectra of Xe in $Ca_xNa_{12-2x}A$ under magic angle spinning. In these simulated spectra we have assumed the fractions of each type of cage in the sample. In Fig. 13, the NMR spectra of Xe in Linde 4A under magic angle spinning, we have assumed a distribution of 40% Ca_0 and 60% Ca_1 cages only. The GCMC simulations of Xe in $Ca_0Na_{12}A$ and $Ca_1Na_{10}A$ alpha cages provide the Xe distribution (relative intensities within one progression) and the Xe_n chemical shifts (peak positions). In Fig. 14, we have assumed a distribution of Ca occupancies: 6% Ca_0, 64% Ca_1, 27% Ca_2 and 2% Ca_3 cages for the high level of Ca^{2+} ion exchange ($x = 1.20$) in order to compare with experiment. The line widths of individual lines used in the simulations in Figs. 13 and 14 were assumed to be the same throughout and a typical value was assumed, based on line shapes under magic angle spinning in pure NaA. All other quantities used in generating the simulated spectrum, that is, the individual values of Xe occupancies of each type of cage, $P(n)$, leading to relative intensities within a progression of Xe_n peaks associated with each cage type, and the individual peak positions or Xe_n chemical shifts associated with each cage type, $[\delta(Xe_n)]_{Ca0}, \ldots, [\delta(Xe_n)]_{Ca3}$, were entirely determined from the GCMC simulations.

Comparison with experiment in Fig. 13 is remarkably good, especially when we consider that a single number, the fraction of Ca_1 cages, is assumed uniformly for all the samples (a)–(d). All other quantities were obtained from the GCMC simulations. The changes in the Intensity(Xe_n) profiles, while varying the overall $\langle n \rangle_{Xe}$ in each of the samples (a)–(d), are predetermined by the individual $\langle n \rangle_{Ca0}$, $\langle n \rangle_{Ca1}$, etc.,

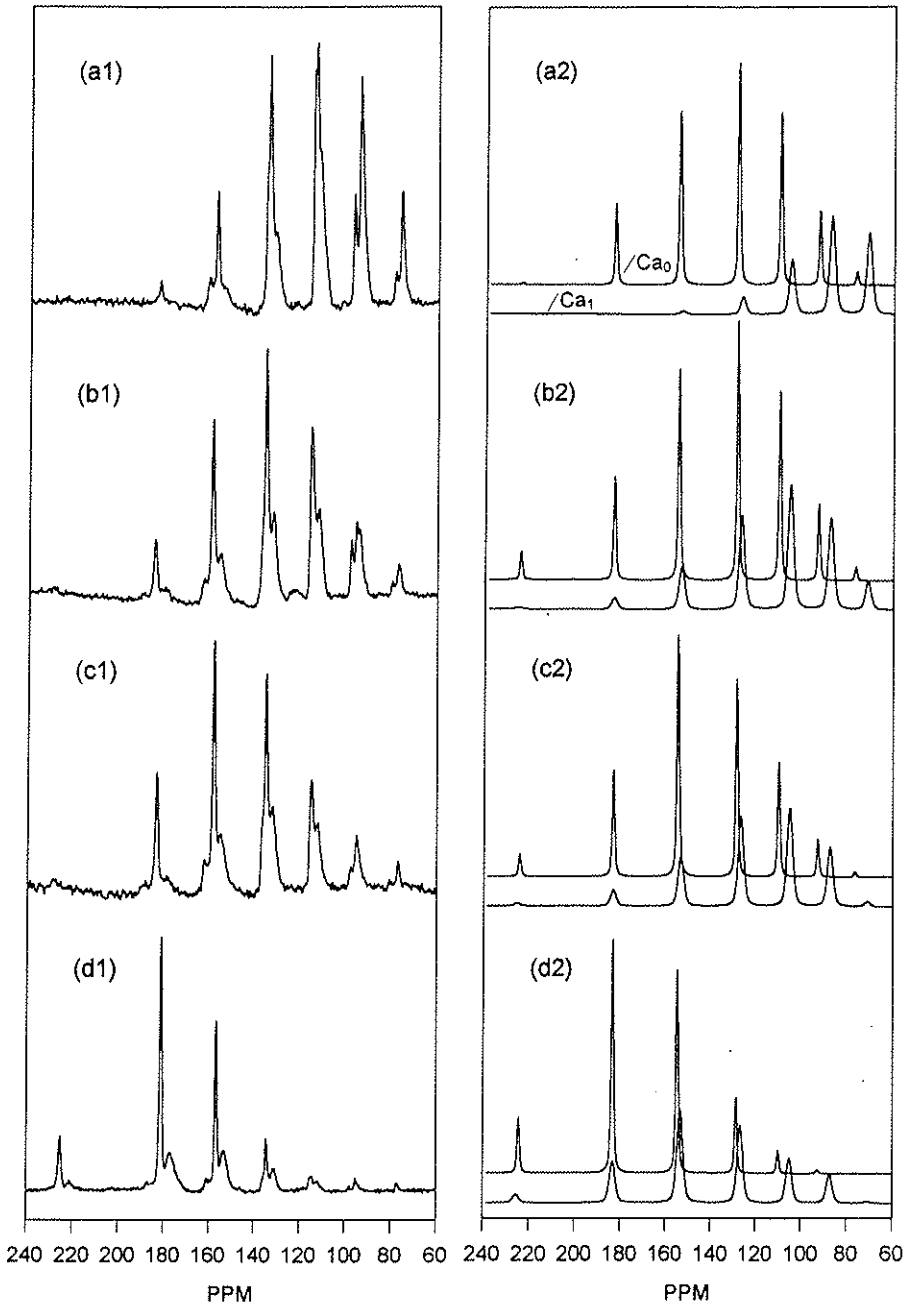

Fig. 13. Simulated spectra of Linde 4*A* under magic angle spinning from GCMC simulations of Xe in $Ca_0Na_{12}A$ and $Ca_1Na_{10}A$ alpha cages, where we have assumed a distribution of 40% Ca_0 and 60% Ca_1 cages only. On the left are the experimental spectra at overall loadings given in Table 2, as published in Ref. [20]. On the right are the spectra predicted from GCMC simulations in this work. The Xe_n chemical shifts and the Xe distribution (relative intensities within one progession) for various loadings are taken from simulations in $Ca_0Na_{12}A$ and $Ca_1Na_{10}A$ cages using parameter set II.

that each cage type is locked into by the GCMC simulations once the Xe chemical potential is set by the overhead gas. In the Ca^{2+} ion exchange experiment, growing in of the cages with higher Ca^{2+} ion content was observed in comparing the two samples of Xe in $Ca_xNa_{12-2x}A$ at a low (an average of 0.60 Ca/cage) and a high level of Ca^{2+} ion exchange (1.20 Ca/cage), under magic angle spinning. The Ca_1 cages, already showing their clearly identifiable progression of Xe_n peaks in the low level of Ca^{2+} ion exchange, become more prominent in the higher level of Ca^{2+} ion exchange. The Xe_n in the Ca_2

cages are barely observable in the former, but have grown in intensity in the latter, where these Ca_2 cages are clearly identifiable. The very small peaks coming from Xe_n in the Ca_3 cages can just barely be located, due to their low intensities. In Fig. 14 the agreement of the simulated spectrum with experiment is very good. Here, too, all that was assumed was the overall $\langle n \rangle_{Xe}$ in the samples. All other values used in the spectral simulation resulted from the grand ensemble averages in the GCMC simulations. With Figs. 13 and 14, we have shown that with the help of GCMC simulations it is possible, at least in this case, to deduce the nature of the cation distribution after cation exchange by using Xe NMR spectroscopy.

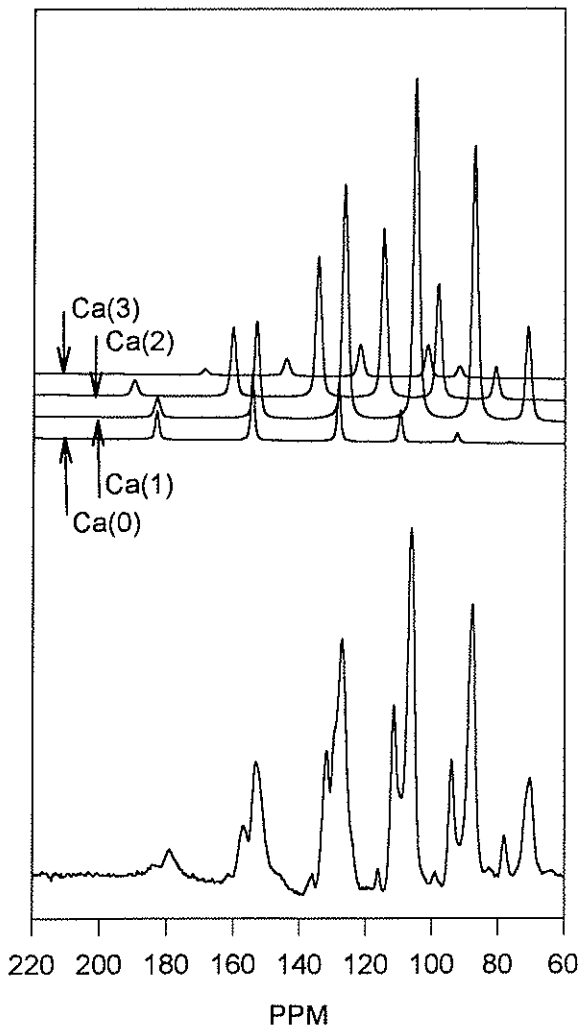

Fig. 14. Simulated spectra of Ca-exchanged Na A from GCMC simulations of Xe in $Ca_0Na_{12}A$, $Ca_1Na_{10}A$, Ca_2Na_8A and Ca_3Na_6A cages, where we have assumed a distribution of 6% Ca_0, 64% Ca_1, 27% Ca_2, and 2% Ca_3 cages. The Xe distribution (relative intensities within one progession) and the Xe_n chemical shifts are from simulations using parameter set II. On the bottom is the experimental spectrum obtained under magic angle spinning for a modest level of Ca-exchange, as published in Ref. [20].

5.3. Sensitivity to the parameters of the simulation

How sensitive are the important results (average chemical shifts of Xe_n and average occupancy of each cage type) obtained from the GCMC simulations to the arrangement of Ca^{2+} ions? For the Ca^{2+} ion positions, we tried both the Ca^{2+} ion coordinates of the Pluth–Smith refined structure for $Ca_5Na_{0.4}A$ and the Adams–Haselden X-ray structure for Ca_5Na_2A in our simulation box. In the Pluth–Smith structure, the Ca^{2+} ion is located more inside the alpha cage while in the Adams–Haselden structure the Ca^{2+} ion is less inside the alpha cage. There are only small differences between the two sets of results for adsorption isotherms, but somewhat more pronounced differences in the chemical shifts (as large as 3 ppm for $Ca_1Na_{10}A$, 9 ppm for Ca_2Na_8A, and 13 ppm for Ca_3Na_6A); the Ca^{2+} ions more inside the alpha cage gave rise to larger chemical shifts in general because the Xe is more exposed to the Ca^{2+} ion in the averaging. The final results we present here used the Pluth–Smith coordinates for Ca_1, Ca_2, and Ca_3, and the Adams–Haselden coordinates for Ca_5 cages. For the $Ca_1Na_{10}A$ cage types, the precise coordinates of the site I position for the Ca^{2+} ion does not have a significant effect on the chemical shifts of the Xe_n ($n = 1,8$).

For the Ca_2Na_8A cage types, the adsorption isotherm has a significant dependence on the chosen configuration of the 2 Ca^{2+} ions due to the large dependence of the induction energy on the configuration of the 2 Ca^{2+} ions. Since there are undoubtedly a distribution of Ca_2 configurations among the Ca_2Na_8A cage types in the zeolite, the minimum energy Ca_2 configuration would not be the appropriate one to use as a typical one for calculating average properties. We used one of the low energy Ca_2 configurations as a typical average configuration. The Xe_n chemical shifts on the other hand, are found to be not particularly sensitive to the choice for the low n occupancies, while the higher n Xe_n chemical shifts are highly sensitive. We have no experimental

observations for Xe_6, Xe_7, or Xe_8 in the Ca_2Na_8A cage types, so it is not possible to check this. The average chemical shifts of all Xe_n are very sensitive to the chosen Ca_3 configuration and the adsorption isotherm for the Ca_3 cages is very sensitive to the chosen Ca_3 configuration. We used the low energy configuration shown in Fig. 3. However, it is difficult to check experimentally whether this is a reasonable choice since the fraction of Xe atoms found in cages containing 3 Ca^{2+} ions is small.

How sensitive are the GCMC results to the potential parameters used for the Lennard–Jones function and the partial charges used in the calculation of the polarization? The adsorption isotherm is rather sensitive to the choice of partial charges for Na, O, Al, Si, and to the choice of the V_{LJ}(Xe–O) and V_{LJ}(Xe–cation) parameters. Here, we adjusted the V_{LJ} by simply scaling down the attractive part using a factor β less than 1.0, starting from the set of parameters for the all-LJ potential used by us previously [18,19]. The adsorption isotherms for Ca A which have been measured by Tsiao et al. [14] and also in our laboratory [23] were used to choose a reasonable β and this assignment was checked against the Xe_n chemical shifts in Na A, given that the set of partial charges is taken from the Mulliken analysis at the 6-311G** basis set. The choice of q_{Ca}/q_{Na} affects the predicted separations between $Ca_xNa_{12-x}A$ and Na A chemical shifts and adsorption isotherms. A larger charge could be chosen to give better agreement with experiment in the Xe chemical shifts in Ca-exchanged cages, but at the same time, this would give worse adsorption isotherms compared to that observed [14,23].

5.4. Consequences of removal of Na(II)

Finally, we consider the possibility that there are some Na(II) ions that may have been removed during Ca^{2+} ion substitution. This would lead to formation of two or more cages interconnected by an open window, which would have led to chemical shifts appropriate to a much larger cavity. For example, in addition to Xe_5 clusters in normal sized alpha cages there would be some Xe_5 clusters found in the double-sized cavity produced from averaging of Xe_n and Xe_{5-n} clusters in adjacent connected alpha cages. We had concluded from the experimental MAS NMR spectra that there was no sign of such double cages in the spectra of Ca^{2+}-exchanged Na A at the low Ca^{2+} substitutions used in this work [20]. We have tested this conclusion by carrying out GCMC simulations in a simulation box of double cages. A double cage was created by replacing one Na(I) and one Na(II) in one cage by a Ca^{2+} ion in site I and replacing one Na(I) and one Na(III) by a Ca^{2+} ion in site I in the adjacent cage. The average chemical shifts of the Xe_1 through Xe_{16} in these double cages are collected. Results are shown in Fig. 15 of an NMR spectrum that has been simulated in a crystallite in which 33% of the alpha cages are participating in double cages. In this simulated spectrum the signals from the Xe_n in the $Na_{12}A$ cages are labeled Xe_n and the signals from the double cages are shown according to their distributions and are numbered 1 through 10. The Xe_{2n} in double cages give rise to average chemical shifts that are 3–13 ppm more deshielded (higher chemical shift) than Xe_n in single alpha cages that contain the same number of Ca^{2+} ions per cage. Furthermore, these double cages have a distribution of occupancies which is different from that of the single cages. Comparison of this spectrum with the experimental spectra suggests that if indeed there had been a small fraction of double cages, the

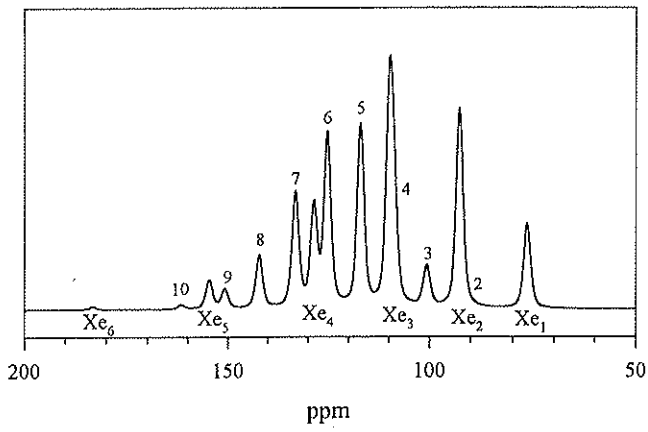

Fig. 15. The spectrum predicted by GCMC simulations for a crystallite with $Ca_1Na_{10}A$ cages, in which 33% of the alpha cages are participating in double cages, i.e., cages in which the Ca^{2+} ion replacement process has removed the Na^+ ion from the shared window. The chemical shifts of the Xe_n from the normal $Ca_0Na_{12}A$ cages are labeled 'Xe_n', whereas the Xe_n from the double cages are labeled with the number of Xe atoms in the double cage. The Xe in the normal $Ca_0Na_{12}A$ cages and the double cages are all in equilibrium with the same gas (i.e., they are at the same chemical potential).

chemical shifts associated with the Xe in the double cages would have been observed, since several additional peaks would appear between the usual Xe_n peaks (in single alpha cages). Clearly, if any double cages had been produced by loss of Na(II) from the 8-ring windows during the Ca^{2+} substitution, the fraction of double cages was much too small to be clearly established experimentally. The absence of the peaks from this predicted spectrum in the experimental spectrum shows that there was no significant loss of Na(II) to Ca^{2+} substitution in our experiments.

Why do we not see more opening up of cages in our experiments? It has been suggested [41,42,70] that in the Ca substitution for Na in Na *A*, the Na(II) sites are less stable than Na(I) sites. Yet at low levels of overall Ca substitution we do not observe in the MAS NMR spectra a preference for loss of Na(II) compared to Na(I). It has been reported that pore opening occurs at 33% exchange of Ca for Na (i.e., Ca_2Na_8A), from adsorption experiments [71]. This does not imply that Na(II) ions are missing from the windows of those alpha cages containing 2 Ca^{2+} ions and $8Na^+$ ions, however. As we have established by the Xe NMR experiments, there is a distribution of cage types even at low levels of substitution in Ca-exchanged Na *A*; co-existing in the crystallite are Ca_0, Ca_1, Ca_2, and Ca_3-containing cages. Thus, at the level of substitution where the average Ca content is Ca_2Na_8A, there would be a very substantial fraction of cages that are Ca_4Na_4A and Ca_5Na_2A types, having open windows, permitting fast Xe exchange among many interconnected cages. It is clear from the studies of Tsiao et al. [14] that many interconnected cages can exist when the average number of Ca^{2+} substitutions reaches $x = 2$ in $Ca_xNa_{12-2x}Si_{12}Al_{12}O_{48}$.

Although we carried out the simulations in the double cages for the specific purpose of confirming whether or not a substantial loss of Na(II) may have occurred, there are some very interesting results that have been revealed by the double cages. The positions of the cations in the double cage simulations were dictated by the following desired properties: They lead to the same average number of Ca and Na per cages as in $Ca_1Na_{10}A$; Na(II) has been removed from the connecting window. Incidentally, there is one Na(III) still present in the double cage. Now we can compare chemical shifts and adsorption isotherms as a function of pore size, while keeping all other factors (number and types and locations of cations, framework structure, Xe chemical potential) the same. (1) Comparing $\delta(Xe_{2n})$ in a single cage vs. $\delta(Xe_n)$ in a double cage shows the dependence of the Xe chemical shift on the pore size at a given loading. We find $[\delta(Xe_n)]_{double} < [\delta(Xe_n)]_{single}$, i.e., the same number of atoms in a larger cage gives a lower chemical shift, except for Xe_1 and Xe_2. (2) Comparing $\delta(Xe_n)$ in a single cage vs. $\delta(Xe_n)$ in a double cage shows the dependence of the Xe chemical shift on the pore size at a given density. We find $[\delta(Xe_{2n})]_{double} > [\delta(Xe_n)]_{single}$; in the double cage, a Xe atom has access to a larger number of Xe atoms, which gives rise to a greater chemical shift. (3) At the identical Xe chemical potential, we find the double cages adsorb 2.584 Xe atoms per alpha cage whereas the single cage in Na *A* adsorbs 1.894 Xe atoms per alpha cage. At the same chemical potential, the single cage in $Ca_1Na_{10}A$ adsorbs 0.96 Xe atoms per alpha cage. That is, the larger pore exhibits an adsorption isotherm that has greater adsorption than the smaller pore, other conditions being kept the same.

5.5. Xe in CaA under fast exchange

Without changing any of the parameters in the potential functions used, Xe under fast exchange in an *A* zeolite has been simulated here. The results for the adsorption isotherm and the Xe chemical shifts as a function of loading in Figs. 10 and 11 are in good agreement with experimental results from this and other laboratories. It was found that the adsorption isotherm could be reproduced even without explicitly including polarization terms, but the Xe chemical shifts are found to be more sensitive to the separation of polarization terms from Lennard–Jones. There is one trend worth noting in the simulations. The Xe chemical shift as a function of loading has a greater curvature (δ_{Xe} increasing faster with $\langle n \rangle_{Xe}$ than linearly) in the GCMC simulations than is found experimentally, as seen in Fig. 11. This curvature becomes evident as soon as the last Na(II) is eliminated, whether polarization is included or not.

The average chemical shift in Na A, averaged over all configurations as if fast exchange could occur, has a less pronounced curvature. The greater curvature predicted than found experimentally in Ca A is therefore associated with the absence of the Na(II) in the windows, leading to closer Xe–Xe interactions between cages. A possible explanation of the discrepancy between the experimental curvature and that resulting from GCMC simulations is the neglect of the Xe–Xe–Xe three-body terms contributions to the potential energy and the chemical shifts. It has been established experimentally that the density coefficient of the chemical shift in liquids is smaller in magnitude than the density coefficient in the dilute gas, not only for ^{129}Xe but for other nuclei such as ^{19}F as well [72]. This means that the contributions of many-body terms to the intermolecular chemical shift is opposite in sign to the two-body term, in general. We had not previously considered the three-body terms in the Xe–Xe contributions to the chemical shifts in zeolites. In the compartmentalized Na A where no more than 8 Xe atoms are in close proximity to each other, we have been able to neglect many-body contributions involving 3 or more Xe atoms. At the highest loadings of Ca A, the Xe–Xe pair distribution function is comparable to that in the bulk liquid and the open network permits a larger sum over three-body terms than in Na A. When the Na(II) ions are no longer in the 8-ring windows that connect adjacent cages (as in Ca_5Na_2 A), the simulated Xe chemical shift rises more sharply from medium loading toward the highest loadings, when compared with the predicted curvature of the averaged Xe chemical shift in Na A.

6. Conclusions

We have found that the partial replacement of monovalent cations by divalent ones requires that the polarization of Xe be explicitly included in describing the potential energy of interaction between the Xe and the zeolite. No set of pairwise additive Lennard–Jones potentials could reproduce the qualitative trends observed experimentally. With increasing Ca^{2+} ion substitution, the qualitative behavior of the $\langle n \rangle_{Xe}$ and the Xe_n chemical shifts for each type of cavity could be reproduced by including some polarization (induction) energy. The details of the distributions and the chemical shifts observed in the cation-exchanged zeolite A vary with the parameterization of the electrostatic potential, as might have been expected, but the qualitative trends are preserved with any reasonable set of parameters. This leads to the conclusion that our assignments of the Xe_n progressions to the types of cages with 0, 1, 2, 3 Ca^{2+} ions is correct. The nature of the distribution of Ca^{2+} ions upon Ca^{2+} exchange for $2Na^+$ that we have found here is probably typical of what one might expect in any kind of cation-exchanged zeolites.

In this work, we have had the opportunity to observe directly comparable adsorption isotherms for cages differing by successive substitution of divalent for monovalent ions; all the various types of cages are in equilibrium with the same gas and at the same temperature in the sample; that is, all Xe are at the same chemical potential. Thus, we could compared with each other the results of GCMC simulations at fixed (μ, T, V), using various types of cages, and these could be compared with experiment. We also have directly determined the Xe_n chemical shifts in each of these different cages, providing additional independent tests of the simulations. Each Xe_n explores the inside of one of the various Ca_1Na_{10} A, Ca_2Na_8 A, Ca_3Na_6 A cages and these Xe_n chemical shifts can be compared to Xe_n in Ca_0Na_{12} A cages. Although the choices of partial charges and Lennard–Jones parameters are not unique, we have presented in Tables 4 and 5 (set II) a reasonable set of parameters that provides agreement with detailed Xe NMR experiments in Ca_xNa_{12-2x} A ($x = 0$–5), Na Y, and Na X [65]. We have shown that with the help of GCMC simulations it is possible, at least in this case, to deduce the nature of the cation distribution after partial cation exchange by using Xe NMR spectroscopy. The results presented here serve as a paradigm for future understanding of the relation between the average Xe chemical shift and the type and degree of cation substitution in open network zeolites, where the Xe undergoes fast exchange and reports an average over all types of cages and all types of occupancies resulting in a single chemical shift for the adsorbed phase in equilibrium with a given Xe gas density.

Acknowledgements

This research was supported by the National Science Foundation (Grant CHE95-28066).

References

[1] D.W. Breck, Zeolite Molecular Sieves, Wiley, New York, 1974, pp. 529–588.
[2] D.M. Ruthven, Chem. Eng. Prog. 84 (1988) 42.
[3] H.G. Karge, H.K. Beyer, Zeolite Chemistry and Catalysis, In: P.A. Jacobs, N.I. Jaeger, L. Kubelkova, B. Wichterlova (Eds.), Elsevier, Amsterdam, 1991, p. 43.
[4] G. Engelhardt, U. Lohse, E. Lippmaa, M. Tarmak, M. Mägi, Z. Anorg. Allg. Chemie 482 (1981) 49.
[5] E. Lipmaa, M. Mägi, A. Samoson, G. Engelhardt, A.R. Grimmer, J. Am. Chem. Soc. 102 (1980) 4889.
[6] J. Fraissard, T. Ito, J. Chem. Phys. 76 (1982) 5225.
[7] J. Fraissard, T. Ito, Zeolites 8 (1988) 350.
[8] C. Dybowski, N. Bansal, T.M. Duncan, Ann. Rev. Phys. Chem. 42 (1991) 433.
[9] P.J. Barrie, J. Klinowski, Prog. NMR Spectrosc. 24 (1992) 91.
[10] S.B. Liu, L.J. Ma, M.W. Lin, J.F. Wu, T.L. Chen, J. Phys. Chem. 96 (1992) 8120.
[11] Q. Chen, M.A. Springel-Huet, J. Fraissard, M.L. Smith, D.R. Corbin, C. Dybowski, J. Phys. Chem. 96 (1992) 10914.
[12] S.B. Liu, B.M. Fung, T.C. Yang, E.C. Hong, C.T. Chang, P.C. Shih, F.H. Tong, T.L. Chen, J. Phys. Chem. 98 (1994) 4393.
[13] B. Boddenberg, M. Hartmann, Chem. Phys. Lett. 203 (1993) 243.
[14] C. Tsiao, D.R. Corbin, C. Dybowski, J. Phys. Chem. 94 (1990) 867.
[15] G. Engelhardt, M. Hunger, H. Koller, J. Weitkamp, Zeolites and Related Microporous Materials: State of the Art 1994, In: J. Weitkamp, H.G. Karge, H. Pfeifer, W. Hölderich (Eds.), Elsevier, Amsterdam, 1994, p. 421.
[16] M. Hunger, G. Engelhardt, J. Weitkamp, Zeolites and Related Microporous Materials: State of the Art 1994, In: J. Weitkamp, H.G. Karge, H. Pfeifer, W. Hölderich (Eds.), Elsevier, Amsterdam, 1994, p. 725.
[17] C.J. Jameson, A.K. Jameson, R.E. Gerald II, A.C. de Dios, J. Chem. Phys. 96 (1992) 1676.
[18] C.J. Jameson, A.K. Jameson, B.I. Baello, H.M. Lim, J. Chem. Phys. 100 (1994) 5965.
[19] C.J. Jameson, A.K. Jameson, R.E. Gerald II, H.M. Lim, J. Chem. Phys. 103 (1995) 8811.
[20] A.K. Jameson, C.J. Jameson, A.C. de Dios, E. Oldfield, R.E. Gerald II, G.L. Turner, Solid State Nucl. Magn. Reson. 4 (1994) 1.
[21] J.J. Pluth, J.V. Smith, J. Am. Chem. Soc. 102 (1980) 4704.
[22] J. Guemez, S. Velasco, Am. J. Phys. 55 (1987) 154.
[23] C.J. Jameson, A.K. Jameson, R.E. Gerald II, A.C. de Dios, J. Chem. Phys. 96 (1992) 1690.
[24] C.J. Jameson, H.M. Lim, J. Chem. Phys. 103 (1995) 3885.
[25] C.J. Jameson, A.K. Jameson, H.M. Lim, J. Chem. Phys. 104 (1996) 1709.
[26] G.B. Woods, J.S. Rowlinson, J. Chem. Soc., Faraday Trans. 2 85 (1989) 765.
[27] G.B. Woods, D. Phil. Thesis, Oxford University, 1989.
[28] P. Coppens, M.B. Hall (Eds.), Electron Distributions and the Chemical Bond, Plenum, New York, 1982.
[29] M.A. Spackman, R.F. Stewart, Chemical Applications of Molecular Electrostatic Potentials, In: P. Politzer, D. Truhlar (Eds.), Plenum, New York, 1981, p. 407.
[30] M.A. Spackman, R.F. Stewart in Methods and Applications of Crystallographic Computing, In: S.R. Hall, T. Ashida (Eds.), Oxford Univ. Press, 1984, p. 302.
[31] M.A. Spackman, H.P. Weber, J. Phys. Chem. 92 (1988) 794.
[32] E. Preuss, G. Linden, M. Peuckert, J. Phys. Chem. 89 (1985) 2955.
[33] E.C. de Lara, T.N. Tan, J. Phys. Chem. 80 (1976) 1917.
[34] E. Dempsey, Molecular Sieves, Society of Chemical Industry, London, 1968, p. 293.
[35] P. Demontis, G.B. Suffritti, S. Bordiga, R. Buzzoni, J. Chem. Soc., Faraday Trans. 91 (1995) 525.
[36] P. Demontis, S. Yashonath, M.L. Klein, J. Phys. Chem. 93 (1989) 5016.
[37] S. Yashonath, P. Demontis, M.L. Klein, Chem. Phys. Lett. 153 (1988) 551.
[38] S. Yashonath, P. Demontis, M.L. Klein, J. Phys. Chem. 951 (1991) 588.
[39] B. Barrachin, E.C. de Lara, J. Chem. Soc., Faraday Trans. 2 82 (1986) 1953.
[40] P. Demontis, G.B. Suffriti, S. Bordiga, R. Buzzoni, J. Chem. Soc., Faraday Trans. 91 (1995) 525.
[41] K. Ogawa, M. Nitta, K. Aomura, J. Phys. Chem. 82 (1978) 1655.
[42] K. Ogawa, M. Nitta, K. Aomura, Zeolites 1 (1981) 169.
[43] G.K. Moon, S.G. Choi, H.S. Kim, S.H. Lee, Bull. Korean Chem. Soc. 13 (1992) 317.
[44] G.K. Moon, S.G. Choi, H.S. Kim, S.H. Lee, Bull. Korean Chem. Soc. 14 (1993) 356.
[45] E.C. de Lara, R. Kahn, A.M. Goulay, J. Chem. Phys. 90 (1989) 7482.
[46] E. Cohen de Lara, J. Vincent-Geisse, J. Phys. Chem. 80 (1976) 1922.
[47] D.M. Ruthven, R.I. Derrah, J. Chem. Soc., Faraday Trans. 1 71 (1975) 2031.
[48] R.I. Derrah, D.M. Ruthven, Can. J. Chem. 53 (1975) 996.
[49] P. Broier, A.V. Kiselev, E.A. Lesnik, A.A. Lopatkin, Russ. J. Phys. Chem. 42 (1968) 1350.
[50] H. Kono, A. Takasaka, J. Phys. Chem. 91 (1987) 4044.
[51] P.R. van Tassel, H.T. Davis, A.V. McCormick, Mol. Phys. 73 (1991) 1107.
[52] D.M. Razmus, C.K. Hall, AIChE J. 37 (1991) 769.
[53] R.J. Neddendriep, J. Colloid Interface Sci. 28 (1968) 293.
[54] J.L. Soto, P.W. Fisher, A.J. Glessner, A. Myers, J. Chem. Soc., Faraday Trans. 1 77 (1981) 157.
[55] P.R. van Tassel, H.T. Davis, A.V. McCormick, J. Chem. Phys. 98 (1993) 8919.

[56] V. Bosacek, J. Dubsky, Collect. Czech. Chem. Commun. 40 (1975) 3281.
[57] A.V. Kiselev, P.Q. Du, J. Chem. Soc., Faraday Trans. 2 77 (1981) 1.
[58] P.R. van Tassel, H.T. Davis, A.V. McCormick, J. Chem. Phys. 98 (1993) 8919.
[59] A.J. Stone, Chem. Phys. Lett. 83 (1981) 233.
[60] A.J. Stone, M. Alderton, Mol. Phys. 56 (1985) 1047.
[61] P.W. Fowler, A.D. Buckingham, J. Chem. Phys. 79 (1983) 6426.
[62] F. Vigne-Maeder, A. Auroux, J. Phys. Chem. 94 (1990) 316.
[63] S. Huzinaga, Gaussian Basis Sets for Molecular Calculations, Elsevier, Amsterdam, 1984.
[64] C.P. Herrero, J. Phys. Chem. 97 (1993) 3338.
[65] C.J. Jameson, A.K. Jameson, R.E. Gerald II, H.M. Lim, J. Phys. Chem. 101 (1997) 8418.
[66] K.T. No, J.S. Kim, Y.Y. Huh, W.K. Kim, M.S. Jhon, J. Phys. Chem. 91 (1987) 740.
[67] V.L. Alexander, E.C. de Lara, Mol. Phys. 88 (1996) 1399.
[68] J.J. Pluth, J.V. Smith, J. Am. Chem. Soc. 105 (1983) 1192.
[69] J.M. Adams, D.A. Haselden, J. Solid State Chem. 51 (1984) 83.
[70] K.O. Koh, H. Chon, M.S. Jhon, J. Catal. 98 (1986) 126.
[71] T. Takaishi, Y. Yatsurugi, A. Yusa, T. Kuratomi, J. Chem. Soc., Faraday Trans. 1 71 (1975) 97.
[72] C.J. Jameson, Chem. Rev. 91 (1991) 1375.